| | | | | | |
|---|---|---|---|---|---|
| Tanaka M, Ikeda K, Suganami T, Komiya C, Ochi K, Shirakawa I, Hamaguchi M, Nishimura S, Manabe I, Matsuda T, Kimura K, Inoue H, Inagaki Y, Aoe S, Yamasaki S, Ogawa Y. | Macrophage-inducible C-type lectin underlies obesity-induced adipose tissue fibrosis. | Nat. Commun. | 5 | 4982 | 2014 |
| Nakagawa Y, Sakuma T, Nakagata N, Yamasaki S, Takeda N, Ohmuraya M, Yamamoto T. | Application of oocyte cryopreservation technology in TALEN-mediated mouse genome editing. | Exp Anim. | 63 | 349-55 | 2014 |
| Giordano M, Roncagalli R, Bourdely P, Chasson L, Bufferne M, Yamasaki S, Beyaert R, van Loo G, Auphan-Anezin N, Schmitt-Verhulst AM, Verdeil G. | The tumor necrosis factor alpha-induced protein 3 (TNFAIP3, A20) imposes a brake on anti tumor activity of CD8 T cells. | Proc. Natl. Acad. Sci. USA | 111 | 11115-20 | 2014 |
| Phongsisay V, Iizasa E, Hara H,Yamasaki S. | LMIR5 extracellular domain activates myeloid cells through Toll-like receptor 4. | Mol. Immunol. | 62 | 169-77 | 2014 |
| Hattori Y, Morita D, Fujiwara N,Mori D, Nakamura T, Harashima H, Yamasaki S, Sugita M. | Glycerol monomycolate is a novel ligand for the human, but not mouse macrophage inducible C-type lectin,Mincle. | J. Biol. Chem. | 289 | 15405-12 | 2014 |
| Yamasaki S. | Clec12a: Quieting the Dead. | Immunity | 40 | 309-11 | 2014 |
| Kawai Y, Ouchida R, Yamasaki S, Dragone L, Tsubata T, Wang JY. | LAPTM5 promotes lysosomal degradation of intracellular but not the cell surface CD3ζ. | Immunol. Cell Biol. | 92 | 527-34 | 2014 |

| | | | | | |
|---|---|---|---|---|---|
| Roncagalli R, Hauri S, Fiore F, Liang Y, Chen Z,Sansoni A, Kanduri K, Joly R, Malzac A, Lahdemaki H,Lahesmaa R, Yamasaki S, Saito T, Mallisen M, Aebersold R, Gstaiger M, Malissen B. | Quantitative proteomic analysis of signalosome dynamics in primary T cells identifies the surface receptor CD6 as a LAT-independent TCR signaling hub. | Nat. Immunol. | 15 | 384-92 | 2014 |
| Toyonaga K, Miyake Y, Yamasaki S. | Characterization of the receptors for mycobacterial cord factor in Guinea pig. | PLoS One | 9 | e88747 | 2014 |

Cell Host & Microbe
Article

# Olfactory Plays a Key Role in Spatiotemporal Pathogenesis of Cerebral Malaria

Hong Zhao,[1,14] Taiki Aoshi,[2,7,14] Satoru Kawai,[8,14] Yuki Mori,[6] Aki Konishi,[1] Muge Ozkan,[1] Yukiko Fujita,[1] Yasunari Haseda,[7] Mikiko Shimizu,[1] Masako Kohyama,[3] Kouji Kobiyama,[2,7] Kei Eto,[9] Junichi Nabekura,[9] Toshihiro Horii,[10] Tomoko Ishino,[11] Masao Yuda,[11] Hiroaki Hemmi,[4] Tsuneyasu Kaisho,[4] Shizuo Akira,[5] Manabu Kinoshita,[12] Koujiro Tohyama,[13] Yoshichika Yoshioka,[6,15] Ken J. Ishii,[2,7,15] and Cevayir Coban[1,15,*]

[1]Laboratory of Malaria Immunology
[2]Laboratory of Vaccine Science
[3]Laboratory of Immunochemistry
[4]Laboratory of Immune Regulation
[5]Laboratory of Host Defense
[6]Laboratory of Biofunctional Imaging
Immunology Frontier Research Center (IFReC), Osaka University, 3-1 Yamadaoka, Suita, Osaka 565-0871, Japan
[7]Laboratory of Adjuvant Innovation, National Institute of Biomedical Innovation (NIBIO), 7-6-8 Saito-Asagi, Ibaraki, Osaka 567-0085, Japan
[8]Departments of Tropical Medicine and Parasitology, Dokkyo University School of Medicine, Mibu, Tochigi 321-0293, Japan
[9]Division of Homeostatic Development Unit, National Institute for Physiological Sciences, 38 Nishigonaka Myodaiji, Okazaki, Aichi 444-8585, Japan
[10]Department of Molecular Protozoology, Research Institute for Microbial Diseases, Osaka University, 3-1 Yamadaoka, Suita, Osaka 565-0871, Japan
[11]Department of Medical Zoology, Mie University School of Medicine, Mie, Tsu 514-0001, Japan
[12]Osaka Medical Center for Cancer and Cardiovascular Diseases, Higashinari-ku, Osaka 537-8511, Japan
[13]Laboratory for Nano-neuroanatomy, Iwate Medical University, 19-1 Uchimaru, Morioka, Iwate 020-8505, Japan
[14]These authors contributed equally to this work
[15]Co-senior authors; these authors contributed equally to this work
*Correspondence: ccoban@biken.osaka-u.ac.jp
http://dx.doi.org/10.1016/j.chom.2014.04.008

## SUMMARY

Cerebral malaria is a complication of *Plasmodium falciparum* infection characterized by sudden coma, death, or neurodisability. Studies using a mouse model of experimental cerebral malaria (ECM) have indicated that blood-brain barrier disruption and CD8 T cell recruitment contribute to disease, but the spatiotemporal mechanisms are poorly understood. We show by ultra-high-field MRI and multiphoton microscopy that the olfactory bulb is physically and functionally damaged (loss of smell) by *Plasmodium* parasites during ECM. The trabecular small capillaries comprising the olfactory bulb show parasite accumulation and cell occlusion followed by microbleeding, events associated with high fever and cytokine storm. Specifically, the olfactory upregulates chemokine CCL21, and loss or functional blockade of its receptors CCR7 and CXCR3 results in decreased CD8 T cell activation and recruitment, respectively, as well as prolonged survival. Thus, early detection of olfaction loss and blockade of pathological cell recruitment may offer potential therapeutic strategies for ECM.

## INTRODUCTION

Cerebral malaria (CM) is a severe complication of malaria infection in humans caused by *P. falciparum* parasites and characterized by sudden clinical symptoms such as convulsions and coma with high rates of death or long-term disabilities (Idro et al., 2010; Taylor et al., 2004). Early diagnosis of CM is not easy, as it presents with nonspecific symptoms, often resulting in the manifestation of disease at a time point when CM treatment is less effective. Therefore, early, quick, and cheap diagnosis of CM that allows timely interventions has been needed.

A mouse model of CM using *P. berghei* ANKA (*Pb*A) parasites (experimental cerebral malaria, ECM) has widely been used to understand the pathogenesis of CM (Langhorne et al., 2011). Although the brain is a privileged site that prevents the entry of exogenous pathogens where tight endothelial cells form the blood-brain barrier (BBB), ECM is believed to result from multiple reasons such as BBB breakage, followed by inflammatory responses and cell accumulation in the brain. Indeed, a large number of studies suggest that various cells, mostly leukocytes in high numbers, accumulate in the brain vessels where infected red blood cells (iRBCs) and parasite-specific pathogenic CD8 T cells crossprimed by CD8α+ dendritic cells (DCs) play a critical role in ECM pathogenesis (Baptista et al., 2010; Haque et al., 2011; Howland et al., 2013; Lundie et al., 2008; McQuillan et al., 2011). Moreover,

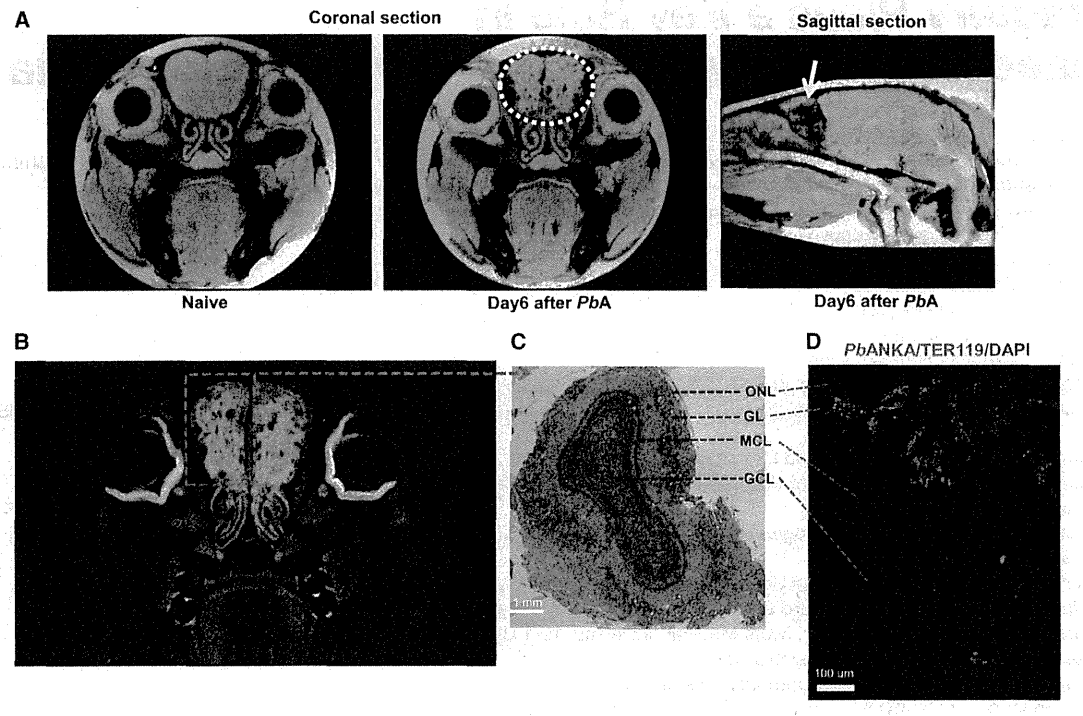


**Figure 1. Ultra-High-Field MRI Identifies OLF Bulb as a Vulnerable Location for *Pb*A Parasites**
C57BL/6 mice were infected with $10^6$ *Pb*A parasites.
(A) 11.7 T MRI of coronal and sagittal sections of mice heads (FLASH T2-star signals, naive v.s. infected). White dotted circle in coronal section and white arrow in sagittal section correspond to OLF bulb.
(B) DWI of coronal section of mouse head on day 6. Gray dotted rectangle and arrow point to HE staining in (C). The images in (A) and (B) are representative of at least five animals.
(C) Histology of coronal section of OLF on day 6 after infection. Hypodense regions correspond to several bleeding sites by HE staining (scale bar, 1 mm). ONL (OLF nerve layer), GL (glomerular layer), MCL (mitral cell layer), GCL (granule cell layer).
(D) IHC of OLF section on day 6. Red, TER119+ erythrocytes; green, GFP-*Pb*A parasites; blue, nuclei (DAPI). Scale bar, 100 μm.
See also Figures S1 and S2.

recent studies have reported CD11c expression on activated CD8 T cells during *Pb*A infection, yet their precise role is not studied well (Tamura et al., 2011). Although these systemic as well as local events for the dysfunction of BBB are well studied, whether the initial brain injury and BBB disruption occur in blood vessels of the whole brain simultaneously or there is a particular location that allows brain to become permissive to iRBC and pathological events has not been fully addressed.

In this study, we investigated the spatiotemporal regulation of pathophysiological and immunological mechanisms of murine CM, using combination of two powerful imaging techniques, an ultra-high-field 11.7 T MRI and multiphoton microscopy (MP). We elucidated the underlying mechanisms where brain became permissive during systemic infection with *Pb*A parasites. We found that the olfactory bulb (OLF), composed of unique capillary structures, serves as a suitable environment for parasites as well as cell migration, and is the first place to sense malaria infection and permit "crosstalk" between the brain and the activated immune system. This links the OLF with loss of smell, high fever, astrocytes, CCL21, CCR7, CXCR3, and CD11c+ CD8 T cells.

## RESULTS

### Ultra-High-Field MRI Imaging Identifies Olfactory Bulb as Location of Microbleeding in the Brain during ECM

To study changes in mouse brain and visualize ECM-related pathology, we performed ultra-high-field 11.7 T MRI (Mori et al., 2011). Six days after *Pb*A infection when specific ECM symptoms such as disorientation and paralysis begin, 11.7 T MRI displayed dark but clear spots in the bilateral OLF (Figure 1A, coronal section), while no other parts of the brain, including cerebrum or cerebellum, showed such spots (Figure 1A, sagittal section). When diffusion-weighted images (DWI) were obtained, details of the OLF region were more evident and remarkably similar to the histological details, where hypodense regions correspond to the bleedings by hematoxylin and eosin (H&E) staining (Figures 1B and 1C). Immunohistochemistry (IHC) also confirmed that bleeding (TER119+ erythrocytes) and GFP-*Pb*A parasites were present in the same area of OLF and were as deep as the granular cell layer (GCL) (Figure 1D). Additional MRI at earlier time points did not detect changes earlier than day 6 postinfection (see Figure S1B available online). Furthermore, several MRI images after the onset of symptoms showed

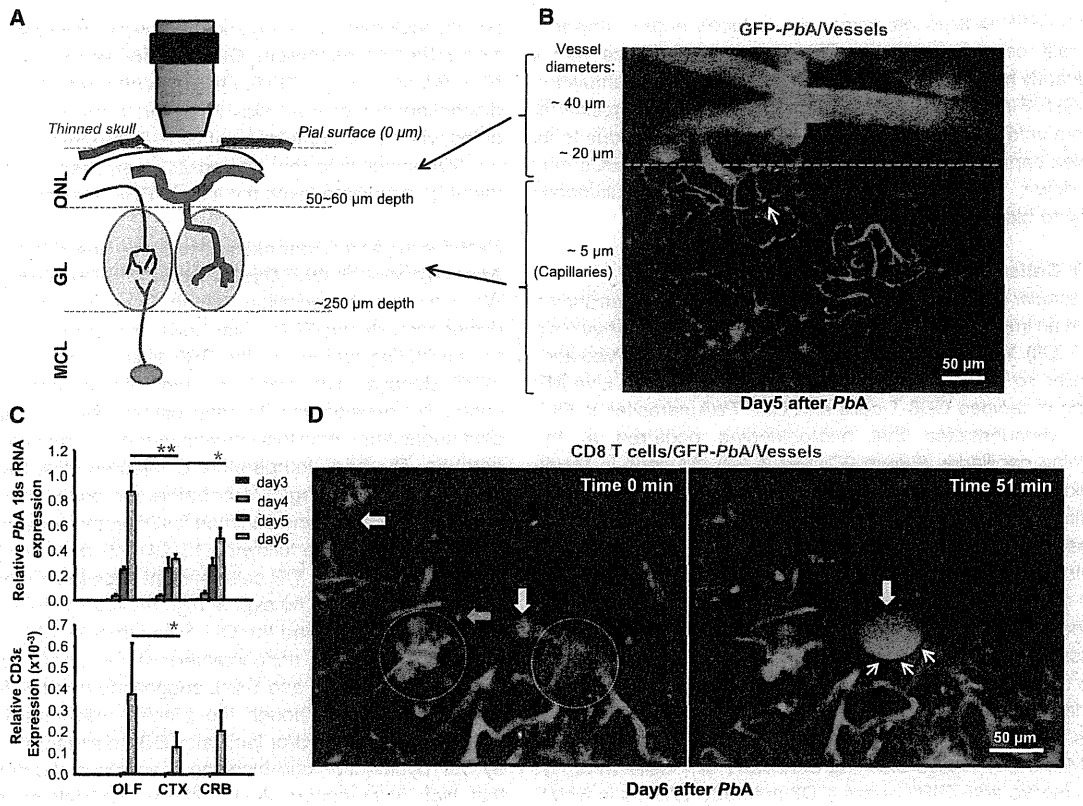


**Figure 2. Intravital Multiphoton Imaging of OLF Bulb during Infection**

(A) Schematic representation of MP microscopy through the thinned-skull of dorsal OLF bulb. The depth of the images is ~150 μm from the pial surface in which capillaries (red, diameter <5 μm) in the GL are visualized. Larger vessels (surface arteries and arterioles, diameter ~20–40 μm) are located in the ONL.

(B) A representative snapshot intravital MP image from WT mouse OLF bulb on day 5 after GFP-*Pb*A infection, related to Movie S1. White arrow shows GFP parasites attached/occluded to the blood vessel labeled with red TRITC-Dextran. Gray line separates bigger vessels and capillaries. Scale bar, 50 μm.

(C) *Pb*A parasite load and CD3ε (pan-T cell surface marker) were quantified by qPCR using primers specific for *Pb*A 18S rRNA and CD3ε on days 3, 4, 5, and 6 after infection in the OLF, cortex, and cerebellum. Results are presented as relative mRNA units (mean ± SE, n = 3 for days 3, 4, and 5 and n = 8 for day 6). *$p < 0.05$ and **$p < 0.01$ for infected versus noninfected mice by Mann-Whitney test.

(D) Fresh microbleeding in OLF. Representative snapshot images (0 and 51 min time point) on day 6 after infection, related to Movie S2. Red, vessels (red TRITC-Dextran); green, GFP-*Pb*A (green arrow); blue, CD8 T cells (anti-CD8 Ab, white arrow). Red areas in gray circles show already-bled regions, yellow arrows show the angular vessels where fresh bleeding will occur, and white arrows show leaked blood vessel indicating fresh bleeding occurred, on the right image.

See also Movie S1, Movie S2, Movie S3, and Movie S4.

different degrees of hemorrhages in the OLF, perhaps implying progressive disease symptoms (Figure S2). However, there was no clear evidence of microhemorrhages in other parts of the brain, even the heavy bleeding occurred in OLF (Figure S2). Furthermore, mice infected with lethal parasites, *P. yoelii*L (*Py*L), had no microbleedings in their OLF (Figure S3A). It is therefore reasonable that our ultra-high-field MRI setting enabled the identification of OLF as a vulnerable area during *Pb*A infection, where bleedings could easily occur compared with other parts of the brain.

### Intravital Multiphoton Imaging of Parasites within OLF Trabecular Small Vessels

We next investigated why and how bleedings occur, including possible involvement of the BBB disintegration, from the OLF during ECM. The OLF is composed of trabecular small vessel structures, which are high in density and oriented in different directions (radially and tangentially). These complex vessels, together with neuron and glial cells, make synaptic interactions in glomeruli and may serve as a scaffold environment for neuronal cell migration in the tissue (Bovetti et al., 2007; Danielyan et al., 2009). To examine whether this unique vessel architecture could be a "weak spot" for iRBC and infection-related events, OLF was visualized by intravital MP microscopy. MP imaging of rodent OLF bulb has previously been performed as deep as GL (~150 μm) which are rich in capillaries (Figure 2A) (Chaigneau et al., 2003; Petzold et al., 2008; Sawada et al., 2011). We performed thinned-skull surgery over the dorsal OLF bulb to maintain tissue intact (Sawada et al., 2011). Live images of OLF vessels showed this region has anatomically complex capillary architecture (diameter <5 μm) (Petzold et al., 2008) and is suitable for the adhesion/occlusion of circulating iRBC, shown as GFP signals expressed in *Pb*A parasites, 5 days after infection (Figure 2B; Movie S1). As seen in Movie S1, the speed

of some GFP-labeled parasites was reduced and/or stopped, eventually causing occlusion. This was in accordance with a significantly higher parasite load as well as T cells' accumulation in the OLF (Figure 2C). Taken together, these results suggest that OLF is a unique area for ECM pathogenesis, possibly due to its complex capillary architecture, whereby circulating iRBCs may slow down, attach, and/or become sequestered, ultimately leading to bleeding.

**CD8 T Cells Traffic via the Blood Vessels in OLF**

Intravascular accumulation of CD8 T cells in the brain was shown to have an important role in the pathogenesis of ECM (Miyakoda et al., 2008). We examined if CD8 T cells could be observed and/or related to microbleeding by intravital MP imaging. Live MP imaging of labeled CD8 T cells and GFP-*Pb*A parasites in OLF clearly demonstrated that microbleeding occurred at the branching capillaries (Figure 2D; Movie S2). As seen in Movie S2, red dextran-labeled capillary structures were altered (red dye almost leaked into tissue). Importantly, CD8 T cells were increased in numbers and "crawling" back and forth in the vessels during the development of ECM (Figure 2D; Movie S2, Movie S3, and Movie S4), and some were associated around the bled regions (Movie S2). Those CD8 T cells in the OLF could be passively moving during unstable blood flow in the terminal phase of ECM; however, our constructed 3D movie in the relatively larger vessels (around 10 μm) clearly indicated that CD8 T cells attached vessels and actively crawling along the vessel wall (Movie S3). These crawling behaviors of T cells were not due to in vivo anti-TCRβ or anti-CD8 antibody labeling in which the same antibody had no effect on T cells of naive mice (Movie S4; data not shown). Rather, activated T cells accumulated in the OLF capillaries starting day 5 and highly increased in numbers with crawling behaviors (Movie S4). Together, these live OLF images indicate that accumulated iRBC with increased and crawling CD8 T cells might leak out of the vessel via microbleeding of the OLF capillaries.

**Olfactory Function Is Destroyed during ECM**

Given the above findings that microbleeding occurs in OLF during ECM, we hypothesized that the OLF function (smell) would be affected, because OLF contains OLF nerves that form a complex physiological synapse for odors. To assess OLF function, we performed a simple buried food test (BFT) (Yang and Crawley, 2009). OLF function was significantly impaired as early as day 4 after infection, as determined by the delayed time to find buried food (Figure 3A), compared with mice that are resistant to ECM such as BALB/c or *Rag2*$^{-/-}$ mice or mice infected with lethal *Py*L parasites (Figure 3B). Thus, olfaction loss might allow the prediction of manifestations of ECM such as bleeding in the OLF and potential loss of BBB integrity.

To evaluate whether the olfaction loss directly correlated with the loss of BBB integrity, Evans-blue dye was injected into mice at early time points (days 3–6) after infection and blue dye extravasation into brain tissues were monitored. In accordance with MP imaging observations where iRBC slowed down and stopped in the vessels, blue dye extravasation into tissue appeared from the OLF as early as day 5 after infection, while the whole brain was blue on day 6 or 7 (Figure 3C). The BBB is restrictive due to tight junctions (TJs), and proteins such as zonula occludens-1 (ZO-1) and ZO-1 were indicated to be localized in the OLF epithelium, OLF sensory neurons, and OLF bulb MCL (Miragall et al., 1994). On day 6 after infection, significant discontinuation of ZO-1 was observed in the MCL, which coincided with the accumulation of GFP-*Pb*A parasites (iRBC) (Figure 3D), suggesting that altered ZO-1 expression in TJ of OLF might be associated with the loss of BBB integrity during ECM.

**High Fever and Chemokine Storm during ECM Are Associated with OLF Dysfunction and Physical Damage**

We next sought possible factors that contributed to OLF dysfunction during ECM. High fever was shown to be one of the facilitating factors for the BBB loss (Kiyatkin and Sharma, 2009). Because high fever is an important symptom of malarial coma, we developed a thermal camera system that allowed continuous and noninvasive measurement of mouse body temperature. The body temperature of infected mice revealed that high-fever attacks begin 24 hr before the onset of ECM symptoms (around day 5) and continue for 24 hr, then end with thermal loss and death in the following 12–24 hr (Figure 3E; Movie S5). When *Rag2*$^{-/-}$ mice, T/B cell-deficient mice that do not develop ECM, were infected, no sign of high fever throughout the infection was observed, and the OLF was intact by MRI (Figures 3F and S3B). Moreover, mice infected with *Py*L or *P. yoelii*NL had no fever (Figures 3G and S4A), suggesting that the fever could be *Pb*A specific. Although the precise mechanism by which high fever triggers and/or facilitates BBB disintegration followed by OLF dysfunction and bleeding is not clear, the data suggest that high fever occurs 24 hr before ECM-related death and may be correlated to BBB leakage. Of note, elevated systemic serum cytokine levels at day 5 after infection may support the notion that cytokine storm accompanies high fever (Figure S4B).

**CCL21 Is Expressed in OLF at the Early Stage of Infection**

We further investigated other possible factors relevant to olfaction loss. Chemokines are early mediators of inflammation and have increasingly being recognized as contributors in the pathogenesis of fever (Machado et al., 2007). As some chemokines and cytokines have critical roles in the development of ECM, expression levels of several of them were measured in the OLF. CCL21 and CCL19 mRNA and protein levels were highly expressed as early as day 3 after infection in the OLF bulb (Figures 4A and 4B), suggesting the early expression of chemokines, especially CCL21, might be important during ECM.

These results above prompted us to examine whether CCR7 (receptor for CCL21 and CCL19) is involved in the pathology of ECM. We infected WT and littermate *Ccr7*$^{+/-}$ and *Ccr7*$^{-/-}$ mice with *Pb*A and followed their survival. A significant increase in survival among *Ccr7*$^{-/-}$ mice occurred, and death was caused by high parasitemia, with no difference in parasite levels between groups during ECM period (Figure 4C; data not shown). To evaluate whether olfaction in *Ccr7*$^{-/-}$ mice was intact, a BFT was performed and found to be intact (Figure 4D). Interestingly, high fever occurred with a delayed onset in *Ccr7*$^{-/-}$ mice (~48 hr) (Figure 4E) with no signs of bleeding in the OLF at day 6 (Figures S5A and S5B). Evans blue staining gradually occurred about 80% of *Ccr7*$^{-/-}$ mice brains onward of day 8 (Figure S5B). These data suggested that CCR7 has a role in the pathogenesis

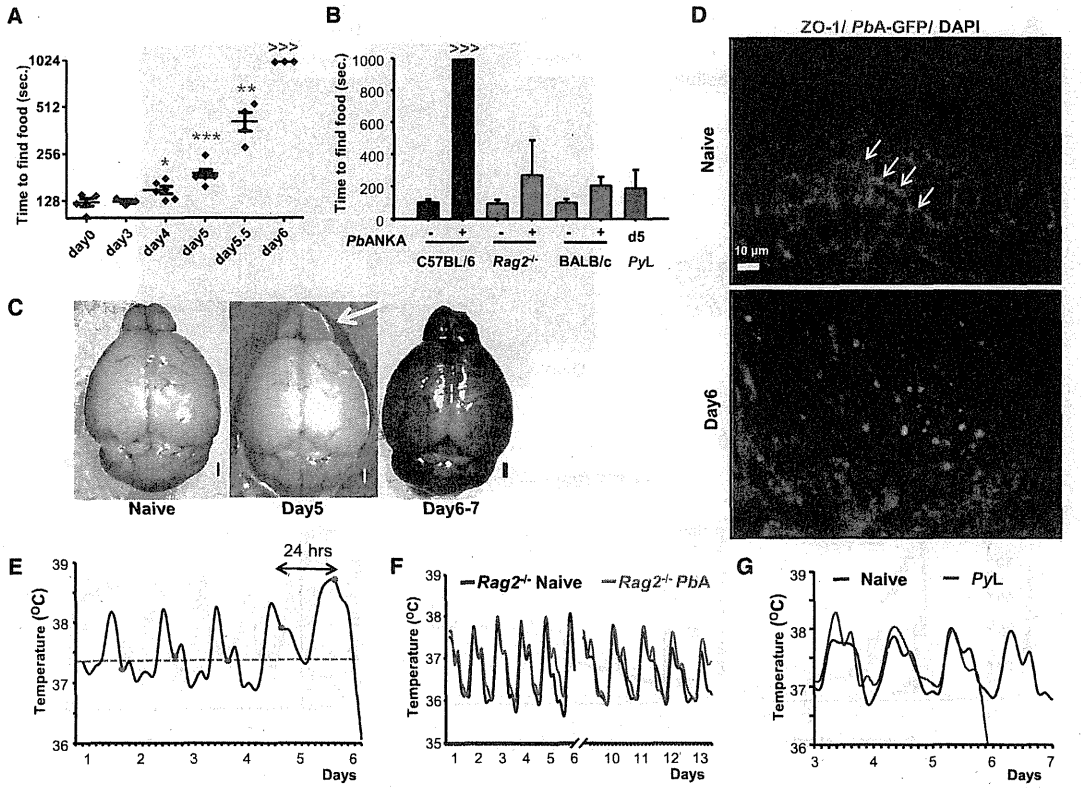


**Figure 3. Olfaction Loss and Fever Occur during ECM**

(A) To assess OLF function, mice were subjected to BFT at the indicated time points. The delay in time to find food is shown in seconds (mean ± SD, n = 4–6 per time point). *p < 0.05, **p < 0.01 and ***p < 0.001 by Student's t test or Mann-Whitney test.

(B) OLF function of naive and *Pb*A- or *Py*L-infected C57BL/6, *Rag2*$^{-/-}$, and BALB/c mice assessed by BFT on day 6 after infection (time to find food is shown in seconds, mean ± SD, n = 5–8 per group). No statistical significance observed between groups by Student's t test. >>> in (A) and (B) shows time greater than 900 s.

(C) Evans blue dye was injected i.v. to assess BBB leakage in naive or infected mice at the indicated time points. Two hours after dye injection, mice were sacrificed, the brains removed, and images captured by dissecting microscopy. White arrow, OLF bulb (scale bar, 1 mm).

(D) IHC of OLF bulbs at the indicated time points. Red, TJ protein ZO-1; green, GFP-*Pb*A; blue, nuclei (DAPI). White arrows show the continuous line of ZO-1 protein around the MCL in naive mice (scale bar, 10 µm).

(E) Thermal camera monitoring of infected C57BL/6 mice, related to Movie S5. Mice movements and fever were continuously recorded in the cages. Mean fever measurements were calculated every 3 hr. Dotted green line shows the median fever level of the same mouse before infection. Red dots show 0–3 a.m. time points for each day.

(F and G) Fever in *Pb*A-infected *Rag2*$^{-/-}$ mice (F) and *Py*L-infected C57BL/6 mice (G) were recorded by thermal camera monitor. Mean fever measurements were calculated every 3 hr.

The data presented in (E)–(G) are representative of at least three infected mice per group. See also Figures S3 and S4.

of ECM, contributing to OLF dysfunction, microbleeding, and high fever.

### CCR7 Expression Is Critical for CD8α DC Priming of CD11c+ CD8 T Cells but Not for Their Migration into Brain

We next investigated underlying mechanism responsible for the increased survival of *Ccr7*$^{-/-}$ mice from ECM. Since CCR7 is important in the migration of immune cells such as DCs and T cells to the secondary lymphoid organs, we examined the recruitment of T cells in the brain. Flow cytometric analysis of immune cells obtained from brains 6 days after infection showed that CD8 T cell accumulation was decreased by 50% in *Ccr7*$^{-/-}$ mice (Figure 5A). A recent report suggested that among the CD8 T cells recruited into the brain, CD11c+ CD8 T cells were highly activated and possibly involved in the pathogenesis by producing IFN-γ and granzyme-B (Tamura et al., 2011). Consistent with this report, we found that CD8 T cells in the brain of infected mice were mostly CD11c+, a population that were remarkably reduced in the infected brains as well as spleens of *Ccr7*$^{-/-}$ mice by percentage, numbers, and activity (Figures 5A, 5B, and 5C, respectively) and secreted IFN-γ (Figure 5D).

We further evaluated whether decreased percentages of CD11c+ CD8 T cells in *Ccr7*$^{-/-}$ mice were caused by defects in the prior priming in spleen. It has been suggested that CD8α+ DCs predispose CD8 T cells in the pathogenesis of ECM, as they can cross prime CD8 T cell responses (Lundie et al., 2008; Piva et al., 2012). We confirmed by infecting basic leucine zipper transcriptional factor ATF-like 3 (*Batf3*)-deficient mice which lack CD8α DCs in the spleen (Murphy et al., 2013)

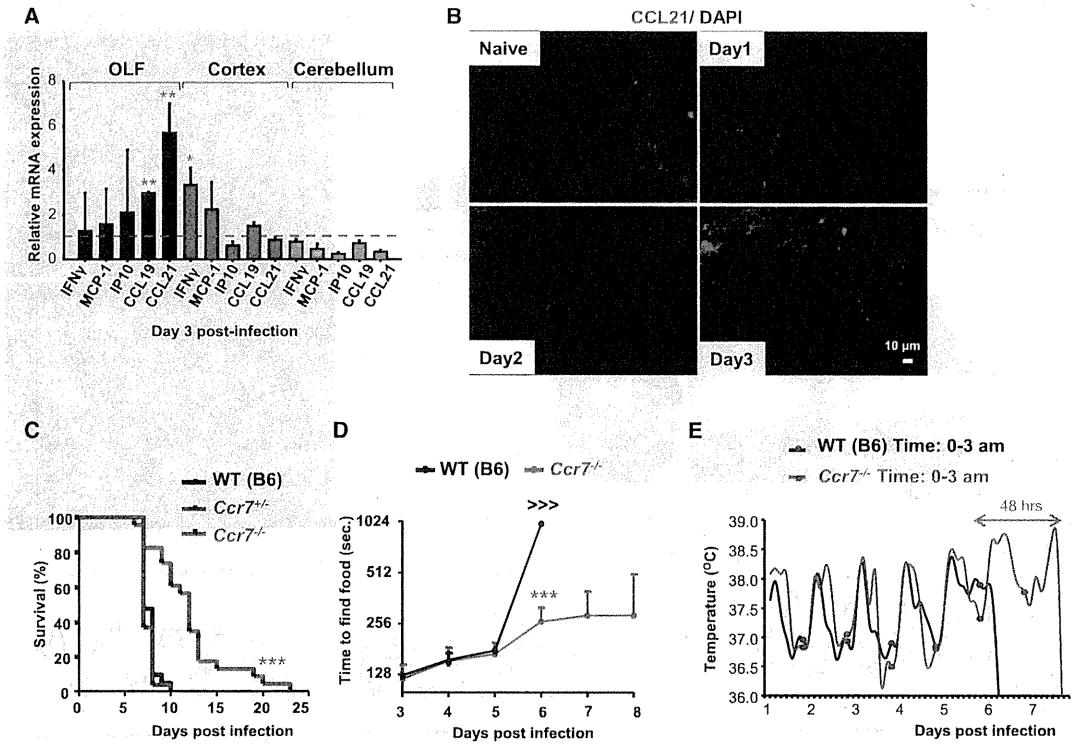


**Figure 4. CCL21 Activity Occurs at OLF Bulb during Infection**

(A) Brain tissues (OLF bulb-cortex-cerebellum) were removed on day 3 postinfection. Expression of indicated chemokine/cytokine mRNA was analyzed by real-time qPCR. Results (mean ± SD) are presented as fold induction compared to naive mice relative mRNA units (n = 3). Red dotted line corresponds to 1. *p < 0.05, **p < 0.01, infected versus noninfected mice by Student's t test.

(B) IHC of OLF bulb sections from infected mice (on days 0–3 postinfection). Red, CCL21; blue, nuclei (DAPI) (scale bar, 10 μm).

(C) Survival curves of WT (C57BL/6, n = 21), *Ccr7*$^{+/-}$ (n = 27) and *Ccr*$^{-/-}$ (n = 23) mice after infection with $10^6$ *PbA*. ***p = 0.0004, log rank (Mantel-Cox) test.

(D) Infected WT and *Ccr7*$^{-/-}$ mice were subjected to BFT. The time to find food is shown in seconds (mean ± SD, n = 4 per time point). ***p < 0.001 by Student's t test. >>> shows time was greater than 900 s.

(E) Continuous fever monitoring of infected WT and *Ccr7*$^{-/-}$ mice. Mean fever measurements were calculated for every 3 hr. Blue and red dots show 0–3 a.m. time points for each day. The data presented are representative of at least three infected animals per group.

See also Figure S5.

that the number of activated CD11c+ CD8 T cells in spleen and their accumulation in brain was significantly impaired in *Batf3*$^{-/-}$ mice with improved survival rate compared to controls (Figures S6A–S6C). However, *Ccr7*$^{-/-}$ mice had almost comparable numbers of CD8α DCs in spleen (Figure S6A); we therefore designed experiments to understand if functional CCR7 expression on CD8α DCs is required for CD8 T cell activation.

### Functional CCR7 Is Required for CD8α DCs' Priming of CD11c+ CD8 T Cells

To seek the role of CCR7 expression on CD8α DC, we purified CD8α DCs from infected *Rag2*$^{-/-}$ mice with intact DCs but no T/B cells (McLellan et al., 2002). Splenic CD8α+ DCs, but not CD8α- DCs, from *Rag2*$^{-/-}$ mice expressed high levels of CCR7 at day 5 after infection (Figure S7A). These CCR7+ CD8α+ DCs were purified (Figure S7B) and adoptively transferred to *Ccr7*$^{-/-}$ mice in which efficiently restored the recruitment of activated CD11c+ CD8 T cells (which originated from *Ccr7*$^{-/-}$ mice) in the brain and accelerated ECM (Figure 5E). Together, these findings suggest that functional CCR7 expression on activated CD8α+ DCs has a critical role in the pathogenesis of ECM, possibly by activating CD11c+ CD8 T cells and their expansion. However, CCR7 expression on CD11c+ CD8 T cells is dispensable for the migration of these cells.

### CCL21 Expressed in OLF Coincides with Activation of Astrocytes and May Be Important for the OLF Migration of CD11c+ CD8 T Cells

The finding that CCR7 is dispensable for the OLF migration of CD11c+ CD8 T cells has implied the importance of CCL21 during priming of CD8 T cells. On the other hand, as CCL21 expression was also observed in OLF from day 3 of infection, we evaluated the possibility that CCL21 might have an additional role on the recruitment of CD8 T cells via an alternative chemokine receptor interaction other than CCR7. Thus, we further analyzed the localization and/or source of CCL21 in the infected OLF. Although it was difficult to address the cell type expressing CCL21, CCL21 staining was confined to the endothelium of inflamed blood vessels where astrocytes are often colocalized (Figure 6A). Astrocytes are specialized cells guarding and sensing blood

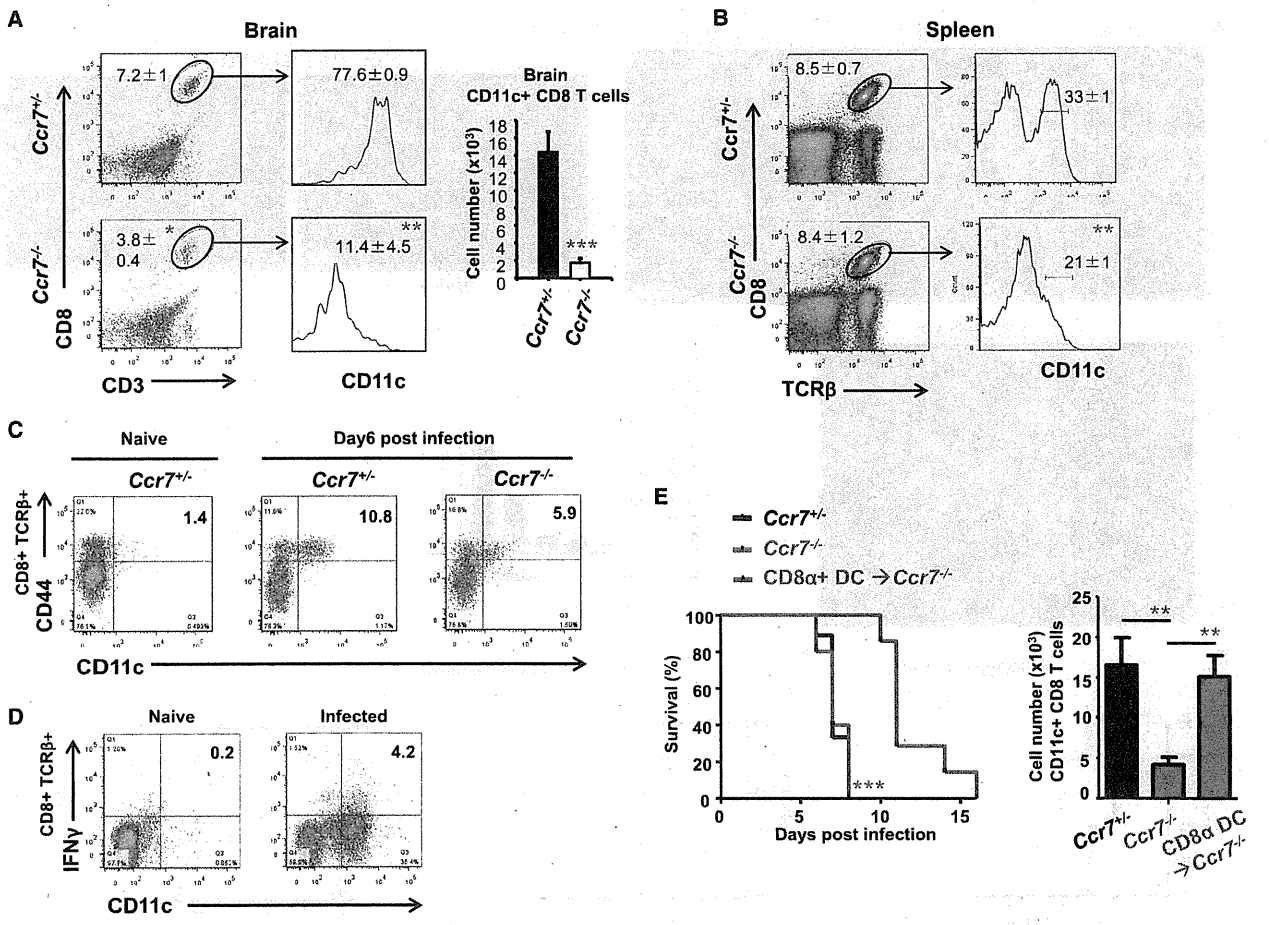


**Figure 5. CCR7 Expression Is Critical for CD8α DC Priming of CD11c+ CD8 T Cells but Not for Their Migration into Brain**

WT and *Ccr7*$^{-/-}$ mice were infected.

(A and B) Flow cytometric analysis of whole brain (A) and spleen (B) cells on day 6 postinfection. Numbers in the insets show percentages of CD8 T cells and their CD11c expression, and the right figure in (A) shows absolute numbers of CD11c+ CD8 T cells in brain (mean ± SEM of four to eight mice per group. *$p < 0.05$, **$p < 0.01$, and ***$p < 0.001$ infected *Ccr7*$^{-/-}$ versus infected *Ccr7*$^{+/-}$ mice by Mann-Whitney test).

(C) Activation status of CD11c+ CD8 T cells in spleen of WT and *Ccr7*$^{-/-}$ mice was determined by CD44 surface staining.

(D) Intracellular staining of IFN-γ secreting CD11c+ CD8 T cells in spleens of WT mice.

(E) Enriched CD8α DCs from infected *Rag2*$^{-/-}$ spleens were adoptively transferred to *Ccr7*$^{-/-}$ mice and infected with *Pb*A, and survival was monitored. Survival curves of *Ccr7*$^{+/-}$ (n = 9), *Ccr7*$^{-/-}$ (n = 7), and transferred *Ccr7*$^{-/-}$ (n = 5) mice after infection are shown. ***$p = 0.0005$, *Ccr7*$^{-/-}$ versus CD8α DC transferred *Ccr7*$^{-/-}$ mice by log rank (Mantel-Cox) test. FACS analysis shows the numbers of accumulated CD11c+ CD8 T cells in brains (mean ± SD of three mice per group). **$p < 0.01$, infected *Ccr7*$^{+/-}$ versus infected *Ccr7*$^{-/-}$ mice and *Ccr7*$^{-/-}$ versus infected CD8α DC transferred *Ccr7*$^{-/-}$ mice by Student's t test.

See also Figures S6 and S7.

vessel changes via their endfeet, and their redistribution in retina was implicated during ECM (Medana et al., 1996). On day 6 after infection, morphological alterations of the astrocytes such as ill-spaced distribution and thick and longer processes were evident in OLF (Figure 6B). Moreover, astrocyte interaction with PECAM-1 was greatly altered. Interestingly, CCL21 staining, especially with its fiber-like structures, was in close interaction with CD8 T cells in the OLF (Figure 6C). Given that CXCR3 has promiscuous interaction with several chemokines including CCL21 especially in microglia and astrocytes (Rappert et al., 2002; van Weering et al., 2010) and is a critical molecule for CD8 T cell migration during ECM (Campanella et al., 2008; Hansen et al., 2007; Van den Steen et al., 2008), to understand if there is a chemotactic interaction between CCL21- and CXCR3-expressing CD11c+ CD8 T cells, we performed in vitro transwell migration assay. The CXCR3+ CD11c+ CD8 T cells dose-dependently migrated toward CCL21 (Figure 6D), suggesting CCL21 may be involved in the recruitment of these cells into OLF during ECM.

### Blocking CCR7-CCL21-CXCR3 Axis Is a Potential Intervention for ECM

Given that CCR7-CCL21 and CCL21-CXCR3 axis may have roles in ECM immunopathology, we evaluated whether CCL21

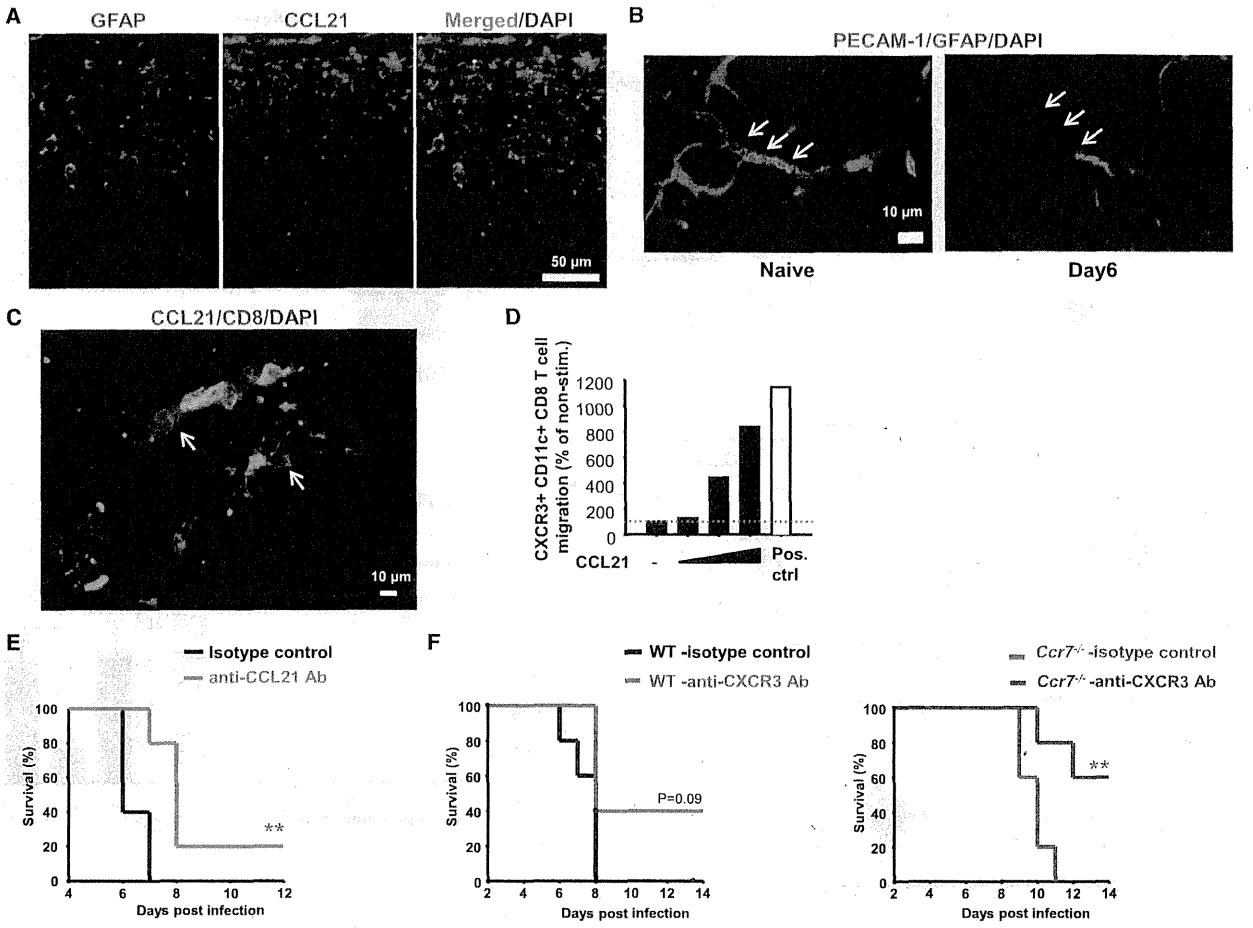


**Figure 6. CCL21 Expressed in OLF Coincides with Astrocyte Activation and May Be Involved in the Migration of CD11c+ CD8 T Cells**

(A) IHC of OLF bulb sections from infected mice on day 6. Green, astrocytes (GFAP); red, CCL21; blue, nuclei (DAPI) (scale bar, 50 μm).

(B) Astrocyte endfeet wrap blood vessels in GL. IHC of OLF bulb GL sections. Green, vessels (PECAM-1); red, astrocytes (GFAP); blue, nuclei (DAPI). White arrows, blood vessels (scale bar, 10 μm).

(C) CD8 T cells associate with CCL21 in OLF. IHC of OLF bulb sections. Green, CCL21; red, CD8 T cells (CD8); blue, nuclei (DAPI) (scale bar, 10 μm). White arrows show fiber-like structures of CCL21 interacting with CD8 T cells.

(D) Migration of purified splenic CD11c+ CXCR3+ CD8 T cells from infected mice in response to recombinant CCL21 (0–2 μg/ml). Human SDF1-α (80 ng/ml) was used as positive control. The migrated cells were counted by flow cytometer, and chemokine-induced migration was normalized to the unstimulated control (gray dotted line) and depicted as percentage.

(E) Mice were i.v. injected daily from the day of infection (0–3 days) with recombinant mouse anti-CCL21 Ab (50 μg per day) and isotype control, and survival was monitored (n = 5 per group, **p < 0.01, log rank [Mantel-Cox] test).

(F) Survival curves of recombinant anti-CXCR3 and isotype control antibody treated groups of WT and *Ccr7*$^{-/-}$ mice after infection. Mice were i.v. injected with antibodies twice at 100 μg per day per mouse on days 4 and 5 after infection. p = 0.09 for isotype control versus anti-CXCR3 Ab group, and **p < 0.01 for *Ccr7*$^{-/-}$ isotype control versus *Ccr7*$^{-/-}$ anti-CXCR3 Ab group by log rank (Mantel-Cox) test (n = 5 per group).

could be exploited as a therapeutic target for the intervention of ECM. Treatment of mice with i.v. anti-CCL21 Ab for the first 3 days of infection led to significantly better survival compared to isotype-control treated mice (Figure 6E). However, anti-CCL21 Ab treatment from day 4 after infection did not have a profound effect on ECM progression (data not shown), suggesting involvement of CCL21 during late stage of ECM might be compromised by the activation of other effector mechanisms. Therefore, we performed combined targeting of CCL21 and CXCR3 by using *Ccr7*$^{-/-}$ mice. Blocking CXCR3 by suboptimal doses of anti-CXCR3 Ab on days 4 and 5 after infection led to significant survival from ECM in *Ccr7*$^{-/-}$ mice as compared to controls (Figure 6F). These data have revealed a proof of concept that combinational blocking of chemokines could be a therapeutic intervention for ECM.

## DISCUSSION

Although brain is severely dysfunctional during ECM due to multiple pathological events such as BBB disruption, vascular

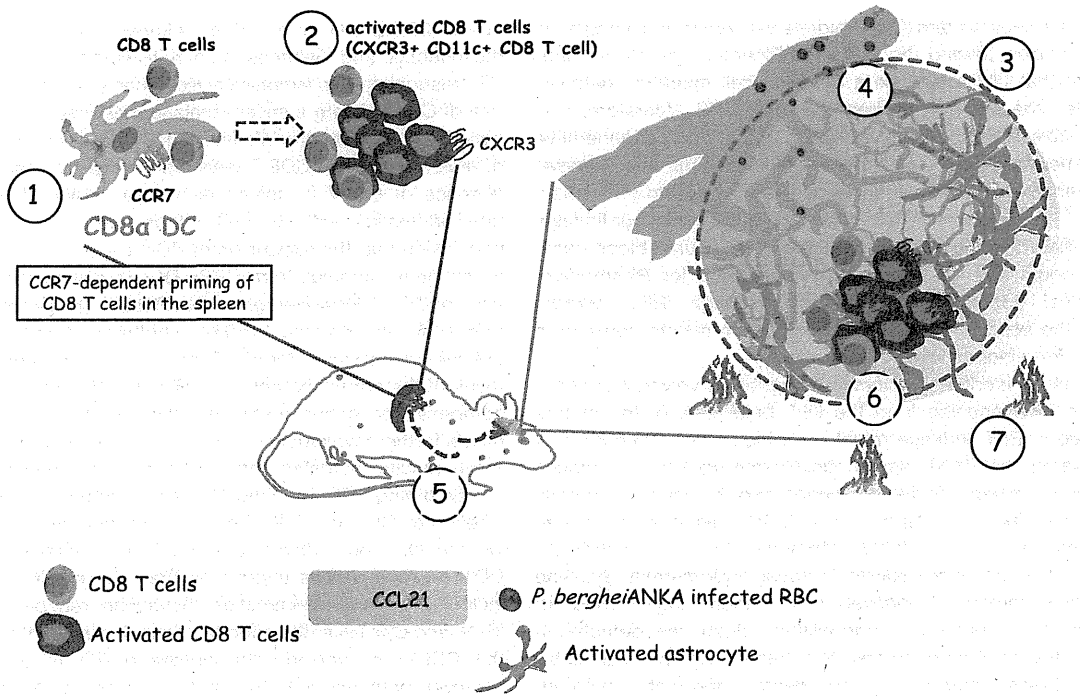


**Figure 7. OLF Bulb Could Be a "Gateway" for *Plasmodium*-Infected Erythrocytes' Accumulation in the Brain**

Once host is infected with *Pb*A parasites, immune cells are activated in periphery such as blood and spleen. Infection-activated CD8α+ DCs in spleen (1) gain ability to crossprime antigens to CD8 T cells via the expression of CCR7. Some of the activated CD8 T cells become effector phenotype by expressing CD11c and CXCR3 (2). These activated immune cells, iRBC, or parasite products are sensed by astrocytes and their surrounding endfeet around the vessels in the OLF glomeruli (3) which possibly induce CCL21 secretion from astrocytes (4), and having a part in opening the BBB gateway to immune cells. Activated CD8 T cells migrate specifically to OLF bulb, where CCL21 and various other effector molecules are secreted (5 and 6), leading to fever and bleeding at OLF (7).

leakage, and immune cell accumulation (especially CD8 T cell infiltration), the exact location at and method by which brain is disrupted are poorly understood. In the current study, we have identified in mice that the OLF region is a vulnerable location for vascular leakage during ECM in which this discovery could only be possible by using an ultra-high-field MRI in combination with MP live imaging microscopy. We further identified that there is an early symptom, olfaction loss, before the onset of coma. Given that even 1 day early detection of malarial coma could increase treatment success dramatically, this previously unnoticed, truly overlooked location and detection of olfaction loss during malaria infection may provide early, cheap, and easy diagnosis of ECM. In search for the underlying mechanism(s) of pathology of ECM via OLF, we found that CCL21 possibly secreted from OLF astrocytes might have a role for the recruitment of pathological CD11c+ CD8 T cells into brain (Figure 7). We further extended this potential function of CCL21 into a therapeutic strategy by blocking chemokine-receptor interactions when the early symptom of ECM, olfaction loss, was evident.

An interesting question is why is the OLF bulb the first place affected by *Plasmodium* parasites? The OLF is composed of very dense capillaries oriented in different directions (radially and tangentially) that exhibit a network of TJ with the thin astrocyte endfeet surrounding the vessel, creating a BBB "guardian." This restricts the flux of substances between the blood and neuronal tissue, maybe via the TJ's capability to transmit information between astrocytes (Chen et al., 2013; Whitman et al., 2009). In the current study, the ONL, blood vessel scaffold around the GL and as deep as MCL was targeted by iRBC or parasite-related events. At present, we do not know what parasite or related factors might contribute to this; however, the TJ network (e.g., ZO-1) might be targeted and possibly disintegrated during ECM. It is possible that perivascular astrocyte endfeet, which are rich in GL and MCL, sense changes in the vessels (De Saint Jan and Westbrook, 2005; Petzold et al., 2008), even when the peripheral parasite burden was very low. Previous studies have reported in cortex that postcapillary venules (labeled with anti-CD14) and/or arteriolar vasoconstriction play a dominant role in ECM pathogenesis (Cabrales et al., 2010; Nacer et al., 2012). Although PECAM-1 staining of OLF vessels seem to be altered in our study, whether there is a differential role for different anatomical vessel structures of OLF needs to be further investigated.

The OLF bulb is known as a dynamic location for OLF nerve projections, especially chemosensations. OLF nerves initiate from the nasal mucosa and terminate in the OLF bulb through the cribriform plate. Lymphatic and blood vessels surround these nerves through which molecules, cells and even pathogens can gain access to brain parenchyma (Danielyan et al., 2009). Recent studies revealed that neuronal cells from the

central nervous system (CNS) migrate via nerves and along brain blood vessels toward the OLF bulb (Bovetti et al., 2007), suggesting that OLF could be a dynamic cell migration gateway between the external environment and CNS. Therefore, it is reasonable that patients suffering from neurodegenerative Alzheimer's or Parkinson's disease and autoimmune diseases experience OLF dysfunction as an early symptom (Mesholam et al., 1998; Strous and Shoenfeld, 2006). Similarly, our findings imply that these dense and directionally structured blood capillaries could also be a suitable environment for *Plasmodium* parasites' adhesion/occlusion—even though iRBC migrate inside the vessels—and these consecutive events could be a reason for olfaction loss.

This study identified factors that might be involved in preceding the BBB opening from the OLF bulb. One of the factors involved in BBB leakage might be a high fever. Although it is speculated that there should be thermoregulation in mouse models of malaria similar to murine sepsis models, currently there have been no reports of a febrile response in mouse malarias (Lamb et al., 2006). Moreover, ECM, in contrast to human infection, is considered to cause hypothermia. By using a thermal camera, a relatively simple technology developed recently (T.A. and K.J.I., unpublished data), we detected a distinct fever period occurring 24 hr before the final manifestation of disease, thermal loss, and death. Importantly, the fever period correlated with severe olfaction loss. Given that the circadian rhythm of mice prevents accurate fever measurement at a single time point, it is not surprising that previous studies could only measure final thermal loss at the final stage of disease. We concluded that systemic and local cytokine/chemokine storm might cause high fever in mice, similar to human CM cases, and probably had the major role in the loss of BBB integrity. Importantly, lack of high fever in *Rag2*$^{-/-}$ mice and in lethal and nonlethal *Py* infections may confirm that fever is associated with ECM and might be related to BBB leakage. However, the mediators causing fever during ECM and their direct role on BBB disruption are currently unknown. The scientific understanding of the mechanism of fever and its relation to cytokinesis have only been performed by using bacterial products such as LPS and LPS challenge models in which fever is known to correlate well with the cytokines IL-1β and TNF-α (Netea et al., 2000). In contrast, there is a lack of information and direct correlation in murine malaria that these very same cytokines would be elevated and cause malarial fever. Clearly, this area needs further investigation.

Astrocytes are common CNS-residing cells essential for regulating blood flow and maintaining the BBB. Astrocytes are also important in immune defense of the CNS by expressing a wide variety of chemokines during physiological and pathological conditions (de Haas et al., 2007; Medana et al., 1996). Furthermore, astrocytes increase CCL21 expression in response to CNS injury and infection (Lalor and Segal, 2010; Noor et al., 2010). An increased CCL21 expression in the OLF, specifically in GL where high numbers of astrocytes are present, led us to study *Ccr7*$^{-/-}$ mice, because CCR7 regulates CNS lymphocyte trafficking via interactions with its ligands, CCL19 and CCL21 (Noor and Wilson, 2012). In addition, previous studies identified chemokine receptors such as CCR5 and CXCR3 that might be important for cellular migration into the brain (Belnoue et al., 2003a, 2003b; Miu et al., 2008). Although the role of CCR7 in the induction and maintenance of antiviral effector and memory CTL responses was extensively examined (Junt et al., 2004), the role of CCR7 during a severe malaria model such as ECM was not investigated before. We found that expansion and migration of effector CD11c+ CD8 T cells were severely impaired in the absence of CCR7 in spleen as well as brain. However, our detailed analysis with CD8α DCs from *Rag2*$^{-/-}$ mice led to the conclusion that the expansion of CD11c+ CD8 T cells required an antigenic stimulus from CD8α DCs in spleen and the presence of CCR7. However, given that *Batf3*$^{-/-}$ mice could escape from ECM only partially (~50%), whether compensation occur between members of the BATF family in DC development as a result of the combined actions of BATF3, BATF, and BATF2 or compensation occurs between other DC types during ECM, needs further investigation (Murphy et al., 2013). Nevertheless, these results indicated that CD8α DC crosspriming of CD8 T cells during ECM required CCR7 that induces the expansion of effector CD11c+ CD8 T cells, which migrate into the brain via the OLF bulb, finally causing ECM. However, activated CD11c+ CD8 T cells migrate to brain via multiple molecules including several chemokines/chemokine receptors such as IP-10 and CXCR3 at the effector phase. It is evident in our study that CCL21 is involved in the priming of CD11c+ CD8 T cells; however, presence of CCL21 at OLF implied its association for the chemotactic support for T cell migration. The CXCR3 was recognized as an alternative receptor for CCL21, especially in astrocytes and microglia (van Weering et al., 2010), and CCL21was shown to be rapidly increased in the brain after *Toxoplasma* infection and supported T cell migration (Wilson et al., 2009). Therefore, it is plausible that CCL21 might be involved in the migration of CXCR3+ CD8 T cells into OLF. Our in vitro transwell migration assay supports this idea; however, limited effect of anti-CCL21 Ab treatment at the onset of OLF dysfunction (on day 4) might suggest compensation of other mechanisms causing pathology during effector phase of ECM in vivo. Nevertheless, here we show a "proof-of-concept" therapeutic approach that blocking CCL21 and/or combination blockage of CCR7-CCL21-CXCR3 axis could be exploited as a strategy for intervention during ECM.

In summary, this study demonstrates that the OLF bulb is a "weak spot" due to its complex architecture and could be a target for *Plasmodium* parasites which cause ECM. Murine studies have also concluded that immune cells such as pathogenic CD11c+ CD8 T cells enter brain via microbleedings at OLF. The CCL21 in the OLF GL during early infection might be one of the underlying mechanisms for the accumulation of pathogenic CD11c+ CD8 T cells, and CCL21 expression might be a risk factor for the development of ECM (Figure 7). These results provide evidence that OLF functional impairment is a valuable marker for ECM development and early diagnosis. Currently, whether these findings in mice are applicable to humans is unclear. Of note, the symptoms of OLF involvement in humans may differ from mice such as "olfactory hallucinations" (Barresi et al., 2012; Perry et al., 2009). Clearly, tests of olfaction loss and techniques such as improved human OLF MRI imaging (Wang et al., 2011) will be needed in future. Furthermore, OLF bulb as a location may be a useful therapeutic target for CM, as well as for various neuroimmune diseases in humans.

## EXPERIMENTAL PROCEDURES

### Parasites and Mice

Two different *Pb*A lines (with and without GFP) were used (Coban et al., 2007; Ishino et al., 2006; Zhao et al., 2012). The C57BL/6 (CLEA, Osaka, Japan), *Ccr7*$^{-/-}$ (kindly provided by Prof. M. Miyasaka and M.H. Jang (Osaka University) (Förster et al., 1999), and *Batf3*$^{-/-}$ (Jackson Labs) mice were used according to the guidelines of NIBIO and Osaka University.

Wild-type mice were i.v. injected daily with anti-CCL21 antibody or isotype control (50 μg per mouse, Peprotech) for 3 days from the beginning of infection. Alternatively, anti-CXCR3 antibody (LEAF-purified anti-mouse CD183 [CXCR3], 100 μg per mouse, Biolegend) was injected twice on days 4 and 5 after infection.

### Buried Food Test

The BFT was performed as previously described (Yang and Crawley, 2009). Briefly, mice were left without food for 18 hr and were placed in a new cage containing buried food under the bedding. The time when the mouse found the buried food was recorded. The test was stopped at 15 min, and its time was recorded as 900 s (latency score, >>>).

### MRI Brain Imaging

An ultra-high-field 11.7 T MRI scanner (AVANCE-II 500 WB; Bruker BioSpin) was used. Initially, naive live mice and 4% paraformaldehyde (PFA)-fixed dead mice heads were compared, and no significant differences were observed (Figure S1A). Therefore, in continuing experiments, infected and deeply anesthetized mice were fixed in PFA and visualized by MRI. The $T_2$* weighted (FLASH sequence) and DWIs (spin echo sequence) were used to detect bleedings.

### Thinned-Skull Surgery and Multiphoton Imaging

The OLF bulb was visualized in living mice by previously described surgically "thinned-skull" technique (Sawada et al., 2011; Wake et al., 2009). Briefly, the mouse head was immobilized and the skull over the OLF was thinned (~20–30 μm). A metal ring was attached to the skull over the region and kept moist during imaging with a microscope (FV1000MPE, Olympus). OLF vasculature was visualized by tetramethylrhodamine isothiocyanate-dextran (5 mg, Sigma) and T cells by brilliant violet 421 conjugated TCR-β (10 μg, Biolegend) or CD8α (5 μg, Biolegend). A Ti-sapphire laser (MaiTai Hp, Spectral Physics) was tuned to the excitation wavelength 800 nm for T cells and vessels, and a Chameleon laser (Coherent) was tuned to 950 nm for GFP–*Pb*A. Time-lapse imaging of deep OLF regions (507.934 μm[x], 507.934 μm[y], 5 μm[z] per 1.1095 s) was performed by continuous repeated acquisition of fluorescence image stacks comprising 30–80 z planes (acquisition of one-stack image requires ~40–90 s). The typical imaging depth was 80–150 μm (Chaigneau et al., 2003). Each mouse was imaged only once. Imaging data were processed and analyzed using Volocity software.

### Temperature Monitoring

A mouse cage with an in-house thermal monitoring system was developed (T.A., unpublished data and patent pending). A cage was prepared like an incubator, with an environmental temperature controlled at 30°C with a 12 hr light-dark cycle and food and water ad libitum. The back skin temperature was continuously recorded (after removing hair) at 1 min intervals by FLIR b60 thermal camera, and the data were analyzed by QuickPlot software (FLIR Systems, Inc.).

### Assessment of BBB Permeability and Histology

At the indicated time points, mice were injected i.v. with 200 μl 1% of Evans blue dye (Sigma) and 2 hr later brains were removed, washed with PBS, and images taken. In addition, brains were removed and prepared for IHC as reported earlier (Zhao et al., 2012).

### Quantitative Real-Time Reverse Transcription-PCR Analysis

Brain samples were homogenized, total RNA was isolated, and q-PCR was performed as described previously (Zhao et al., 2012).

### Flow Cytometric Analysis

Spleen and brain cells were purified as described before (Coban et al., 2007; Zhao et al., 2012). Cell surfaces were stained for CD11c, CD4, CD8α, CD3, TCRβ, CCR7, CD44, CD11c, and CD11b.

### Transwell Migration Assay

Forty-eight-well transwell plates (5 μm pore size, Costar, Corning Inc.) were used for chemotaxis assay as previously described (Rappert et al., 2002).

### Adoptive Transfer Experiments

Total splenocytes were prepared from *Rag2*$^{-/-}$ mice 5 days after infection with *Pb*ANKA, and splenic CD8α+ DC were enriched with a purity >95% (Figure S5B).

### Statistical Analysis

Differences between two groups were analyzed by using Prism software. The log rank (Mantel-Cox) test was performed for survival curves. $p < 0.05$ was considered statistically significant.

## SUPPLEMENTAL INFORMATION

Supplemental Information includes seven figures, Supplemental Experimental Procedures, and five movies and can be found with this article at http://dx.doi.org/10.1016/j.chom.2014.04.008.

## AUTHOR CONTRIBUTIONS

H.Z. performed IHC staining; A.K. infections, food test, and animal monitoring; Y.F. cell isolation, FACS staining, and qPCR; M.O. intracellular staining and transmigration assay; and M.S. parasitemia counts. H.Z., T.A., and Y.H. performed MP microscopy with help from K.E. and J.N.; M.K. helped FASC analysis; Y.M. and Y.Y. performed MRI; T.I. and M.Y. provided parasite lines; S.K., K.K., T.H., H.H., T.K., S.A., and K.J.I. contributed reagents and scientific advice; C.C., K.J.I., T.A., and Y.Y. wrote the manuscript; C.C. directed overall research.

## ACKNOWLEDGMENTS

We thank Drs. K. Suzuki, W. Ise, and H. Arase (IFReC) for various discussions and support. This study was supported by grants from the Ministry of Education, Culture, Sports, Science and Technology in Japan (KAKENHI—Kiban B 25293100) and the Mochida Memorial Foundation for Medical and Pharmaceutical Research.

Received: December 16, 2013
Revised: March 5, 2014
Accepted: April 11, 2014
Published: May 14, 2014

## REFERENCES

Baptista, F.G., Pamplona, A., Pena, A.C., Mota, M.M., Pied, S., and Vigário, A.M. (2010). Accumulation of Plasmodium berghei-infected red blood cells in the brain is crucial for the development of cerebral malaria in mice. Infect. Immun. *78*, 4033–4039.

Barresi, M., Ciurleo, R., Giacoppo, S., Foti Cuzzola, V., Celi, D., Bramanti, P., and Marino, S. (2012). Evaluation of olfactory dysfunction in neurodegenerative diseases. J. Neurol. Sci. *323*, 16–24.

Belnoue, E., Costa, F.T., Vigário, A.M., Voza, T., Gonnet, F., Landau, I., Van Rooijen, N., Mack, M., Kuziel, W.A., and Rénia, L. (2003a). Chemokine receptor CCR2 is not essential for the development of experimental cerebral malaria. Infect. Immun. *71*, 3648–3651.

Belnoue, E., Kayibanda, M., Deschemin, J.C., Viguier, M., Mack, M., Kuziel, W.A., and Rénia, L. (2003b). CCR5 deficiency decreases susceptibility to experimental cerebral malaria. Blood *101*, 4253–4259.

Bovetti, S., Hsieh, Y.C., Bovolin, P., Perroteau, I., Kazunori, T., and Puche, A.C. (2007). Blood vessels form a scaffold for neuroblast migration in the adult olfactory bulb. J. Neurosci. *27*, 5976–5980.

Cabrales, P., Zanini, G.M., Meays, D., Frangos, J.A., and Carvalho, L.J. (2010). Murine cerebral malaria is associated with a vasospasm-like microcirculatory dysfunction, and survival upon rescue treatment is markedly increased by nimodipine. Am. J. Pathol. *176*, 1306–1315.

Campanella, G.S., Tager, A.M., El Khoury, J.K., Thomas, S.Y., Abrazinski, T.A., Manice, L.A., Colvin, R.A., and Luster, A.D. (2008). Chemokine receptor CXCR3 and its ligands CXCL9 and CXCL10 are required for the development of murine cerebral malaria. Proc. Natl. Acad. Sci. USA *105*, 4814–4819.

Chaigneau, E., Oheim, M., Audinat, E., and Charpak, S. (2003). Two-photon imaging of capillary blood flow in olfactory bulb glomeruli. Proc. Natl. Acad. Sci. USA *100*, 13081–13086.

Chen, Y., Mancuso, J., Zhao, Z., Li, X., Cheng, J., Roman, G., and Wong, S.T. (2013). Vasodilation by in vivo activation of astrocyte endfeet via two-photon calcium uncaging as a strategy to prevent brain ischemia. J. Biomed. Opt. *18*, 126012.

Coban, C., Ishii, K.J., Uematsu, S., Arisue, N., Sato, S., Yamamoto, M., Kawai, T., Takeuchi, O., Hisaeda, H., Horii, T., and Akira, S. (2007). Pathological role of Toll-like receptor signaling in cerebral malaria. Int. Immunol. *19*, 67–79.

Danielyan, L., Schäfer, R., von Ameln-Mayerhofer, A., Buadze, M., Geisler, J., Klopfer, T., Burkhardt, U., Proksch, B., Verleysdonk, S., Ayturan, M., et al. (2009). Intranasal delivery of cells to the brain. Eur. J. Cell Biol. *88*, 315–324.

de Haas, A.H., van Weering, H.R., de Jong, E.K., Boddeke, H.W., and Biber, K.P. (2007). Neuronal chemokines: versatile messengers in central nervous system cell interaction. Mol. Neurobiol. *36*, 137–151.

De Saint Jan, D., and Westbrook, G.L. (2005). Detecting activity in olfactory bulb glomeruli with astrocyte recording. J. Neurosci. *25*, 2917–2924.

Förster, R., Schubel, A., Breitfeld, D., Kremmer, E., Renner-Müller, I., Wolf, E., and Lipp, M. (1999). CCR7 coordinates the primary immune response by establishing functional microenvironments in secondary lymphoid organs. Cell *99*, 23–33.

Hansen, D.S., Bernard, N.J., Nie, C.Q., and Schofield, L. (2007). NK cells stimulate recruitment of CXCR3+ T cells to the brain during Plasmodium berghei-mediated cerebral malaria. J. Immunol. *178*, 5779–5788.

Haque, A., Best, S.E., Unosson, K., Amante, F.H., de Labastida, F., Anstey, N.M., Karupiah, G., Smyth, M.J., Heath, W.R., and Engwerda, C.R. (2011). Granzyme B expression by CD8+ T cells is required for the development of experimental cerebral malaria. J. Immunol. *186*, 6148–6156.

Howland, S.W., Poh, C.M., Gun, S.Y., Claser, C., Malleret, B., Shastri, N., Ginhoux, F., Grotenbreg, G.M., and Renia, L. (2013). Brain microvessel cross-presentation is a hallmark of experimental cerebral malaria. EMBO Mol. Med. *5*, 916–931.

Idro, R., Marsh, K., John, C.C., and Newton, C.R. (2010). Cerebral malaria: mechanisms of brain injury and strategies for improved neurocognitive outcome. Pediatr. Res. *68*, 267–274.

Ishino, T., Orito, Y., Chinzei, Y., and Yuda, M. (2006). A calcium-dependent protein kinase regulates Plasmodium ookinete access to the midgut epithelial cell. Mol. Microbiol. *59*, 1175–1184.

Junt, T., Scandella, E., Förster, R., Krebs, P., Krautwald, S., Lipp, M., Hengartner, H., and Ludewig, B. (2004). Impact of CCR7 on priming and distribution of antiviral effector and memory CTL. J. Immunol. *173*, 6684–6693.

Kiyatkin, E.A., and Sharma, H.S. (2009). Permeability of the blood-brain barrier depends on brain temperature. Neuroscience *161*, 926–939.

Lalor, S.J., and Segal, B.M. (2010). Lymphoid chemokines in the CNS. J. Neuroimmunol. *224*, 56–61.

Lamb, T.J., Brown, D.E., Potocnik, A.J., and Langhorne, J. (2006). Insights into the immunopathogenesis of malaria using mouse models. Expert Rev. Mol. Med. *8*, 1–22.

Langhorne, J., Buffet, P., Galinski, M., Good, M., Harty, J., Leroy, D., Mota, M.M., Pasini, E., Renia, L., Riley, E., et al. (2011). The relevance of non-human primate and rodent malaria models for humans. Malar. J. *10*, 23.

Lundie, R.J., de Koning-Ward, T.F., Davey, G.M., Nie, C.Q., Hansen, D.S., Lau, L.S., Mintern, J.D., Belz, G.T., Schofield, L., Carbone, F.R., et al. (2008). Blood-stage Plasmodium infection induces CD8+ T lymphocytes to parasite-expressed antigens, largely regulated by CD8alpha+ dendritic cells. Proc. Natl. Acad. Sci. USA *105*, 14509–14514.

Machado, R.R., Soares, D.M., Proudfoot, A.E., and Souza, G.E. (2007). CCR1 and CCR5 chemokine receptors are involved in fever induced by LPS (E. coli) and RANTES in rats. Brain Res. *1161*, 21–31.

McLellan, A.D., Kapp, M., Eggert, A., Linden, C., Bommhardt, U., Bröcker, E.B., Kämmerer, U., and Kämpgen, E. (2002). Anatomic location and T-cell stimulatory functions of mouse dendritic cell subsets defined by CD4 and CD8 expression. Blood *99*, 2084–2093.

McQuillan, J.A., Mitchell, A.J., Ho, Y.F., Combes, V., Ball, H.J., Golenser, J., Grau, G.E., and Hunt, N.H. (2011). Coincident parasite and CD8 T cell sequestration is required for development of experimental cerebral malaria. Int. J. Parasitol. *41*, 155–163.

Medana, I.M., Chan-Ling, T., and Hunt, N.H. (1996). Redistribution and degeneration of retinal astrocytes in experimental murine cerebral malaria: relationship to disruption of the blood-retinal barrier. Glia *16*, 51–64.

Mesholam, R.I., Moberg, P.J., Mahr, R.N., and Doty, R.L. (1998). Olfaction in neurodegenerative disease: a meta-analysis of olfactory functioning in Alzheimer's and Parkinson's diseases. Arch. Neurol. *55*, 84–90.

Miragall, F., Krause, D., de Vries, U., and Dermietzel, R. (1994). Expression of the tight junction protein ZO-1 in the olfactory system: presence of ZO-1 on olfactory sensory neurons and glial cells. J. Comp. Neurol. *341*, 433–448.

Miu, J., Mitchell, A.J., Müller, M., Carter, S.L., Manders, P.M., McQuillan, J.A., Saunders, B.M., Ball, H.J., Lu, B., Campbell, I.L., and Hunt, N.H. (2008). Chemokine gene expression during fatal murine cerebral malaria and protection due to CXCR3 deficiency. J. Immunol. *180*, 1217–1230.

Miyakoda, M., Kimura, D., Yuda, M., Chinzei, Y., Shibata, Y., Honma, K., and Yui, K. (2008). Malaria-specific and nonspecific activation of CD8+ T cells during blood stage of Plasmodium berghei infection. J. Immunol. *181*, 1420–1428.

Mori, Y., Umeda, M., Fukunaga, M., Ogasawara, K., and Yoshioka, Y. (2011). MR contrast in mouse lymph nodes with subcutaneous administration of iron oxide particles: size dependency. Magn. Reson. Med. Sci. *10*, 219–227.

Murphy, T.L., Tussiwand, R., and Murphy, K.M. (2013). Specificity through cooperation: BATF-IRF interactions control immune-regulatory networks. Nat. Rev. Immunol. *13*, 499–509.

Nacer, A., Movila, A., Baer, K., Mikolajczak, S.A., Kappe, S.H., and Frevert, U. (2012). Neuroimmunological blood brain barrier opening in experimental cerebral malaria. PLoS Pathog. *8*, e1002982.

Netea, M.G., Kullberg, B.J., and Van der Meer, J.W. (2000). Circulating cytokines as mediators of fever. Clin. Infect. Dis. *31* (*Suppl 5*), S178–S184.

Noor, S., and Wilson, E.H. (2012). Role of C-C chemokine receptor type 7 and its ligands during neuroinflammation. J. Neuroinflammation *9*, 77.

Noor, S., Habashy, A.S., Nance, J.P., Clark, R.T., Nemati, K., Carson, M.J., and Wilson, E.H. (2010). CCR7-dependent immunity during acute Toxoplasma gondii infection. Infect. Immun. *78*, 2257–2263.

Perry, T.L., Pandey, P., Grant, J.M., and Kain, K.C. (2009). Severe atovaquone-resistant Plasmodium falciparum malaria in a Canadian traveller returned from the Indian subcontinent. Open Med. *3*, e10–e16.

Petzold, G.C., Albeanu, D.F., Sato, T.F., and Murthy, V.N. (2008). Coupling of neural activity to blood flow in olfactory glomeruli is mediated by astrocytic pathways. Neuron *58*, 897–910.

Piva, L., Tetlak, P., Claser, C., Karjalainen, K., Renia, L., and Ruedl, C. (2012). Cutting edge: Clec9A+ dendritic cells mediate the development of experimental cerebral malaria. J. Immunol. *189*, 1128–1132.

Rappert, A., Biber, K., Nolte, C., Lipp, M., Schubel, A., Lu, B., Gerard, N.P., Gerard, C., Boddeke, H.W., and Kettenmann, H. (2002). Secondary lymphoid tissue chemokine (CCL21) activates CXCR3 to trigger a Cl- current and chemotaxis in murine microglia. J. Immunol. *168*, 3221–3226.

Sawada, M., Kaneko, N., Inada, H., Wake, H., Kato, Y., Yanagawa, Y., Kobayashi, K., Nemoto, T., Nabekura, J., and Sawamoto, K. (2011). Sensory input regulates spatial and subtype-specific patterns of neuronal turnover in the adult olfactory bulb. J. Neurosci. *31*, 11587–11596.

Strous, R.D., and Shoenfeld, Y. (2006). To smell the immune system: olfaction, autoimmunity and brain involvement. Autoimmun. Rev. *6*, 54–60.

Tamura, T., Kimura, K., Yuda, M., and Yui, K. (2011). Prevention of experimental cerebral malaria by Flt3 ligand during infection with Plasmodium berghei ANKA. Infect. Immun. *79*, 3947–3956.

Taylor, T.E., Fu, W.J., Carr, R.A., Whitten, R.O., Mueller, J.S., Fosiko, N.G., Lewallen, S., Liomba, N.G., and Molyneux, M.E. (2004). Differentiating the pathologies of cerebral malaria by postmortem parasite counts. Nat. Med. *10*, 143–145.

Van den Steen, P.E., Deroost, K., Van Aelst, I., Geurts, N., Martens, E., Struyf, S., Nie, C.Q., Hansen, D.S., Matthys, P., Van Damme, J., and Opdenakker, G. (2008). CXCR3 determines strain susceptibility to murine cerebral malaria by mediating T lymphocyte migration toward IFN-gamma-induced chemokines. Eur. J. Immunol. *38*, 1082–1095.

van Weering, H.R., de Jong, A.P., de Haas, A.H., Biber, K.P., and Boddeke, H.W. (2010). CCL21-induced calcium transients and proliferation in primary mouse astrocytes: CXCR3-dependent and independent responses. Brain Behav. Immun. *24*, 768–775.

Wake, H., Moorhouse, A.J., Jinno, S., Kohsaka, S., and Nabekura, J. (2009). Resting microglia directly monitor the functional state of synapses in vivo and determine the fate of ischemic terminals. J. Neurosci. *29*, 3974–3980.

Wang, J., You, H., Liu, J.F., Ni, D.F., Zhang, Z.X., and Guan, J. (2011). Association of olfactory bulb volume and olfactory sulcus depth with olfactory function in patients with Parkinson disease. AJNR Am. J. Neuroradiol. *32*, 677–681.

Whitman, M.C., Fan, W., Rela, L., Rodriguez-Gil, D.J., and Greer, C.A. (2009). Blood vessels form a migratory scaffold in the rostral migratory stream. J. Comp. Neurol. *516*, 94–104.

Wilson, E.H., Harris, T.H., Mrass, P., John, B., Tait, E.D., Wu, G.F., Pepper, M., Wherry, E.J., Dzierzinski, F., Roos, D., et al. (2009). Behavior of parasite-specific effector CD8+ T cells in the brain and visualization of a kinesis-associated system of reticular fibers. Immunity *30*, 300–311.

Yang, M., and Crawley, J.N. (2009). Simple behavioral assessment of mouse olfaction. Curr. Protoc. Neurosci. *Chapter 8*, Unit 8 24.

Zhao, H., Konishi, A., Fujita, Y., Yagi, M., Ohata, K., Aoshi, T., Itagaki, S., Sato, S., Narita, H., Abdelgelil, N.H., et al. (2012). Lipocalin 2 bolsters innate and adaptive immune responses to blood-stage malaria infection by reinforcing host iron metabolism. Cell Host Microbe *12*, 705–716.

Vaccine 32 (2014) 5295–5300

Contents lists available at ScienceDirect

Vaccine

journal homepage: www.elsevier.com/locate/vaccine

# Hemozoin as a novel adjuvant for inactivated whole virion influenza vaccine

Ryuta Uraki[a], Subash C. Das[b], Masato Hatta[b], Maki Kiso[a], Kiyoko Iwatsuki-Horimoto[a], Makoto Ozawa[c,d], Cevayir Coban[e], Ken J. Ishii[f,g], Yoshihiro Kawaoka[a,b,h,i,*]

[a] Division of Virology, Department of Microbiology and Immunology, Institute of Medical Science, University of Tokyo, Tokyo 108-8639, Japan
[b] Influenza Research Institute, Department of Pathobiological Sciences, University of Wisconsin-Madison, Madison, WI 53711, USA
[c] Laboratory of Animal Hygiene, Joint Faculty of Veterinary Medicine, Kagoshima University, Kagoshima 890-0065, Japan
[d] Transboundary Animal Diseases Center, Joint Faculty of Veterinary Medicine, Kagoshima University, Kagoshima 890-0065, Japan
[e] Laboratory of Malaria Immunology, Immunology Frontier Research Center (IFReC), Osaka University, Osaka, Japan
[f] Laboratory of Adjuvant Innovation, National Institute of Biomedical Innovation, Osaka, Japan
[g] Laboratory of Vaccine Science, IFReC, Osaka University, Osaka, Japan
[h] ERATO Infection-Induced Host Responses Project (JST), Saitama 332-0012, Japan
[i] Department of Special Pathogens, International Research Center for Infectious Diseases, Institute of Medical Science, University of Tokyo, Minato-ku, Tokyo 108-8639, Japan

ARTICLE INFO

*Article history:*
Received 31 January 2014
Received in revised form 27 May 2014
Accepted 22 July 2014
Available online 6 August 2014

*Keywords:*
Influenza virus
Vaccine
Hemozoin
Adjuvant
Antibody

ABSTRACT

Because vaccination is an effective means to protect humans from influenza viruses, extensive efforts have been made to develop not only new vaccines, but also for new adjuvants to enhance the efficacy of existing inactivated vaccines. Here, we examined the adjuvanticity of synthetic hemozoin, a synthetic version of the malarial by-product hemozoin, on the vaccine efficacy of inactivated whole influenza viruses in a mouse model. We found that mice immunized twice with hemozoin-adjuvanted inactivated A/California/04/2009 (H1N1pdm09) or A/Vietnam/1203/2004 (H5N1) virus elicited higher virus-specific antibody responses than did mice immunized with non-adjuvanted counterparts. Furthermore, mice immunized with hemozoin-adjuvanted inactivated viruses were better protected from lethal challenge with influenza viruses than were mice immunized with non-adjuvanted inactivated vaccines. Our results show that hemozoin improves the immunogenicity of inactivated influenza viruses, and is thus a promising adjuvant for inactivated whole virion influenza vaccines.



## 1. Introduction

Despite the worldwide surveillance network of influenza viruses, the incidence and prevalence of influenza are hard to predict, as exemplified by the influenza (H1N1) 2009 pandemic [1,2]. Vaccination stands on the frontlines of influenza infection control: both live attenuated and inactivated influenza vaccines are currently available [3,4]. The live attenuated vaccines are more efficient than inactivated vaccines at inducing the mucosal immune responses that play an important role in combating influenza virus infection [5,6]. However, because of the safety concerns such as the emergence of revertant and/or reassortant viruses, these live vaccines are licensed in a limited number of countries. By contrast, inactivated vaccines have few safety concerns and are globally available. While they efficiently induce humoral immune responses, a high dose (usually 15 μg) of the inactivated vaccine is required to provide adequate immunity [7,8]. Therefore, there is room for improvement in the current influenza vaccines.

Vaccine is generally assessed on the basis of immunogenicity, safety, and costs [9]. To enhance the immunogenicity of the inactivated vaccines, adjuvants, such as aluminum compounds and salts, have been considered [10]. Adjuvants are defined as immune modulators that are added to inactivated vaccines to boost the immune responses, enable the use of lower amounts of antigens, and thus expand the vaccine supply [10,11]. Although most of the inactivated influenza vaccines currently used are injected via the intramuscular or subcutaneous routes, previous studies have shown that intranasal vaccinations induce antibodies more effectively than do intramuscular or subcutaneous vaccinations [12–14]. However, the

* Corresponding author at: Division of Virology, Department of Microbiology and Immunology, Institute of Medical Science, University of Tokyo, 4-6-1, Shirokanedai, Minato-ku, Tokyo, Japan. Tel.: +81 3 5449 5504; fax: +81 3 5449 5408.
*E-mail addresses:* kawaoka@ims.u-tokyo.ac.jp, kawaokay@svm.vetmed.wisc.edu (Y. Kawaoka).

http://dx.doi.org/10.1016/j.vaccine.2014.07.079
0264-410X/

alum compounds that are generally used as adjuvants for intramuscular administration do not enhance the efficacy of intranasal vaccines; therefore, to improve the efficacy of intranasal vaccines, novel intranasal adjuvants are required [15].

Malaria parasites digest hemoglobin in red blood cells, resulting in the production of potentially toxic heme metabolites [16]. To protect themselves from oxidative damage, the parasites polymerize toxic heme enzymatically into a safer insoluble substance, hemozoin [17]. Recently, hemozoin and a chemically identical synthetic version of hemozoin (called β-hematin) have been investigated for their potency as novel adjuvants, and the molecular pathway underlying their immunological function has also been studied. Such studies have demonstrated that purified hemozoin is a non-DNA ligand for Toll-like receptor 9 (TLR9) that may activate innate immune cells via TLR9 [18–20]. This latter point has been a subject of debate, however, because the adjuvant effect of synthetic hemozoin is dependent on MyD88 and not TLR9 [21]. Recently, we reported that hemozoin enhances the protective efficacy of a subcutaneously administered influenza HA split vaccine in a ferret model [22].

We speculated that synthetic hemozoin (hereafter referred to only as hemozoin) could serve as a novel intranasal adjuvant for the inactivated influenza vaccine. Accordingly, here we evaluated the adjuvanticity of hemozoin on the vaccine efficacy of intranasally administered inactivated whole virion influenza vaccines in a murine lethal infection model. The results indicate that hemozoin is a promising adjuvant for inactivated whole virion influenza vaccines.

## 2. Materials and methods

### 2.1. Cells and viruses

Human embryonic kidney HEK293T cells were maintained in Dulbecco's modified Eagle medium (Lonza, Basel, Switzerland) supplemented with 10% fetal calf serum (Invitrogen, Carlsbad, CA). Madin-Darby canine kidney (MDCK) cells were maintained in minimum essential medium (MEM) (Invitrogen) supplemented with 5% newborn calf serum (NCS) (Sigma, St. Louis, MO). All cells were maintained in a humidified incubator at 37 °C in 5% $CO_2$.

A/California/04/2009 (H1N1; Ca04), which is an early isolate of influenza (H1N1) 2009 pandemic viruses, and mouse-adapted Ca04 (MACa04) [23] viruses were propagated in MDCK cells as previously described [24]. A/Vietnam/1203/2004 (H5N1; VN1203) virus, a representative strain of highly pathogenic avian influenza viruses, was grown in MDCK cells and in 10-day-old embryonated chicken eggs to use as challenge viruses and as vaccine and ELISA antigens, respectively. All work involving live VN1203 virus was carried out at the ABSL-3 laboratory of the Influenza Research Institute, UW-Madison, following the protocol designed by Institutional Animal Care and Use Committee (IACUC).

### 2.2. Inactivated influenza virus and adjuvant

To inactivate MDCK cell-propagated Ca04 virus and egg-propagated VN1203 virus, formalin (final concentration, 0.1%) was added to the viruses, which were then incubated at 4 °C for 1 week. The inactivated viruses were purified through a 10–50% sucrose density gradient and resuspended in phosphate-buffered saline (PBS) as described previously [25]. Inactivation of Ca04 viruses was confirmed by passaging them twice in MDCK cells and examining their cytopathic effect; inactivation of VN1203 viruses was confirmed by passaging them twice in embryonated chicken eggs followed by hemagglutination assays.

Synthetic hemozoin, was purified from hemin chloride (>98% pure, Fluka) by using the acid-catalyzed method described previously [21] and was re-suspended in endotoxin-free water with no detectable levels of endotoxin. The synthetic hemozoin concentration was calculated in mM (1 mg of hemozoin in 1 ml of water was equal to 1 mM).

### 2.3. Immunization and protection studies

For the immunization and protection studies with Ca04 virus, six-week-old female BALB/c mice ($n = 13$ per group) were anesthetized with isoflurane and intranasally administered with 50 μl of PBS, 9 mM hemozoin only, inactivated Ca04 only [$5 \times 10^6$ plaque-forming unit (PFU), which corresponds to 0.1 μg when the total amount of viral protein was measured by using a BCA protein assay (Thermo Scientific)], or inactivated Ca04 adjuvanted with 9 mM hemozoin, twice with a 2-week interval between the immunizations. Three weeks after the final administration, three mice from each group were euthanized for collection of bronchoalveolar lavage fluid (BALF) and nasal washes. The remaining mice ($n = 10$ per group) were intranasally challenged with 10-fold 50% mouse lethal doses ($MLD_{50}$) of MACa04 virus. On days 3 and 6 post-challenge, three mice each were euthanized and their lungs were collected, homogenized with MEM containing 0.3% BSA, and examined for virus titers by using plaque assays in MDCK cells. The body weight and survival of the remaining challenged mice ($n = 4$ per group) were monitored daily for 14 days.

For VN1203 virus, four-week-old female BALB/c mice ($n = 16$ per group) were immunized as described above. Two weeks after the last immunization, five mice from each group were euthanized for collection of BALF and nasal washes. The remaining mice ($n = 11$ per group) were challenged with 100 $MLD_{50}$ of VN1203 virus. On days 3 and 6 post-challenge, three mice each were euthanized and their lungs were collected, homogenized with MEM containing 0.3% BSA, and examined for virus titers by using plaque assays in MDCK cells. The body weight and survival of the remaining challenged mice ($n = 5$ per group) were monitored daily for 14 days.

### 2.4. Detection of virus-specific antibodies

Virus-specific antibodies in nasal washes, BALF, and serum were detected by using an ELISA as previously described [25–27]. Briefly, 96-well ELISA plate wells were coated with approximately 0.3 μg (in 50 μl) of purified Ca04 or VN1203 virus treated with disruption buffer (0.5 M Tris–HCl [pH 8.0], 0.6 M KCl, and 0.5% Triton X-100) or sarkosyl, respectively. After incubation of the virus-coated plates with the test samples, virus-specific IgA and IgG antibodies in the samples were detected by using anti-mouse IgA and IgG goat antibodies conjugated to horseradish peroxidase (Kirkegaard & Perry Laboratory Inc., Gaithersburg, MD, Rockland), respectively.

### 2.5. Hemagglutination inhibition assay (HI assay)

To detect HI antibodies against Ca04 and VN1203, an HI assay was performed as described previously [28,29]. Briefly, serum samples were treated with receptor-destroying enzyme (RDE; Denka Seiken Co., Ltd.) by incubating at 37 °C for 16–18 h followed by inactivation at 56 °C for 30 min. One volume of turkey or horse red blood cells (RBCs) was then added to 20 volumes of serum and the sera were incubated for 1 h on ice with intermittent mixing. The samples were then centrifuged at 900 × g for 5 min, and the supernatants were transferred to new tubes for use in the HI assay. Serially diluted sera (2-fold dilutions) were mixed with 4 HA units of virus antigen and incubated with 0.5% turkey RBCs or 1% horse RBCs to determine the extent of hemagglutination inhibition.

### 2.6. Statistical analysis

Statistically significant differences in the virus-specific titers ($P < 0.05$ and $P < 0.01$) and the survival rates of the challenged mice ($P < 0.05$) were assessed by use of a one-way ANOVA followed by a Dunnett's test and Log-rank statistical analysis, respectively.

## 3. Results

### 3.1. Hemozoin enhances influenza virus-specific antibody responses in mice

To examine the effect of hemozoin on antibody responses elicited by immunization with inactivated influenza viruses, we intranasally administered BALB/c mice with hemozoin-adjuvanted inactivated virus (Ca04 or VN1203 virus, $5 \times 10^6$ plaque-forming units (PFU), the total amount of viral protein was 0.1 μg) twice with a 2-week interval between the immunizations. At three or two weeks after the final administration, we examined the antibody responses to the administered Ca04 or VN1203 virus by using an ELISA to measure the amount of IgG in the serum and IgA in the BALF and nasal washes (Fig. 1). Neither IgG nor IgA against Ca04 or VN1203 virus was appreciably detected in any samples from the PBS- or hemozoin-administered mice. Under these conditions, although one mouse immunized with non-adjuvanted inactivated Ca04 (Fig. 1A upper panel) and one mouse immunized with non-adjuvanted inactivated VN1203 virus (Fig. 1B upper panel) produced virus-specific IgG in the serum at a detectable level, all of the mice immunized with hemozoin-adjuvanted inactivated Ca04 ($n = 3$) or VN1203 ($n = 5$) virus elicited significantly higher levels of virus-specific IgG in the serum. We also examined the functional properties of the elicited antibodies by using hemagglutination inhibition (HI) assays. For both the Ca04 and VN1203 viruses, greater HI titers were obtained after vaccination with hemozoin-adjuvanted inactivated viruses than with non-adjuvanted inactivated viruses (Fig. 1A and B upper, right panel), although the titer difference for Ca04 virus between the hemozoin group and the control groups was not statistically significant (Fig. 1A upper, right panel). Of note, although the addition of hemozoin did not enhance IgA production in the nasal washes or BALF of the inactivated Ca04 virus-immunized mice, some of the mice immunized with the hemozoin-adjuvanted inactivated VN1203 virus did produce high levels of virus-specific IgA in their nasal washes and BALF (Fig. 1B lower panels). Taken together, these results indicate that hemozoin enhanced the immunogenicity of inactivated influenza viruses, resulting in more efficient production of virus-specific antibodies.

### 3.2. Hemozoin enhances the efficacy of inactivated influenza vaccine against lethal challenge in mice

To further assess the adjuvanticity of hemozoin, mice immunized twice with hemozoin-adjuvanted inactivated Ca04 or VN1203 virus were challenged with a lethal dose of MACa04 (10 $MLD_{50}$) [23] or VN1203 (100 $MLD_{50}$) virus (Fig. 2). In the MACa04 challenge group, although all of the PBS-administered mice and 75% of the hemozoin-administered or inactivated Ca04 virus-immunized mice died, all of the mice immunized with hemozoin-adjuvanted inactivated Ca04 virus survived (Fig. 2A). Intriguingly, no significant difference was found in Ca04 virus titers in the lungs among the mouse groups tested (Table 1). These results suggest that the adjuvanticity of hemozoin was sufficient to protect mice from lethal challenge with MACa04 virus.

For VN1203 virus, all PBS- and hemozoin-administered and inactivated VN1203 virus-immunized mice died following the lethal challenge (Fig. 2B). By contrast, 60% of the mice immunized with hemozoin-adjuvanted inactivated VN1203 virus survived although mice of all groups experienced body weight loss (Fig. 2B). In accordance with the results of the MACa04 virus challenge, the addition of hemozoin to inactivated VN1203 virus immunization did not affect the virus titers in the lungs of VN1203 virus-challenged mice (Table 2). These results suggest that hemozoin enhanced the vaccine efficacy of the inactivated influenza viruses by modulating host responses, but not by directly inhibiting virus replication. Overall, these results suggest that hemozoin is a promising adjuvant for inactivated influenza vaccines.

**Table 1**
Virus titers in the lungs of immunized mice challenged with mouse-adapted Ca04 virus.[a]

| Immunization | Day after challenge | Virus titer (mean $\log_{10}$ PFU ± SD/g) in: lungs |
|---|---|---|
| PBS | 3 | 8.1 ± 0.03 |
| | 6 | 6.5 ± 0.3 |
| Hemozoin | 3 | 8.2 ± 0.03 |
| | 6 | 6.6 ± 0.06 |
| Inactivated Ca04 virus | 3 | 8.1 ± 0.2 |
| | 6 | 5.7 ± 1.0 |
| Hemozoin-adjuvanted inactivated Ca04 virus | 3 | 8.0 ± 0.2 |
| | 6 | 6.2 ± 0.4 |

[a] Mice were intranasally immunized twice with the indicated agents (50 μl per mouse) and challenged with 10 $MLD_{50}$ of MACa04 virus (50 μl per mouse) 3 weeks after the final immunization. Lungs were collected from mice ($n = 3$) on days 3 and 6 after challenge and examined for virus titers by use of plaque assays in MDCK cells.

**Table 2**
Virus titers in the lungs of immunized mice challenged with VN1203 virus.[a]

| Immunization | Day after challenge | Virus titer (mean $\log_{10}$ PFU ± SD/g) in: lungs |
|---|---|---|
| PBS | 3 | 6.3 ± 0.2 |
| | 6 | 6.3 ± 0.2 |
| Hemozoin | 3 | 6.6 ± 0.2 |
| | 6 | 6.3 ± 0.2 |
| Inactivated VN1203 virus | 3 | 6.7 ± 0.3 |
| | 6 | 5.6 ± 0.4 |
| Hemozoin-adjuvanted inactivated VN1203 virus | 3 | 6.4 ± 0.3 |
| | 6 | 6.0 ± 0.4 |

[a] Mice were intranasally immunized twice with the indicated agents (50 μl per mouse) and challenged with 100 $MLD_{50}$ of VN1203 virus (50 μl per mouse) 4 weeks after the final immunization. Lungs were collected from mice ($n = 3$) on days 3 and 6 after challenge and examined for virus titers by use of plaque assays in MDCK cells.

## 4. Discussion

Here, we examined the effect of an adjuvant candidate, hemozoin, on the vaccine efficacy of inactivated whole virion influenza vaccines against lethal challenge in a mouse model. Significantly better virus-specific antibody responses were induced by hemozoin-adjuvanted inactivated virus than by inactivated viruses (Fig. 1). We further demonstrated that the hemozoin-adjuvanted inactivated viruses protected mice from lethal challenges more efficiently than did their non-adjuvanted counterparts with no effect of virus titers in the lungs (Fig. 2, Tables 1 and 2). These results indicate that hemozoin is a promising candidate as an effective adjuvant for inactivated whole virion influenza vaccines.

We observed significantly higher levels of IgA specific for VN1203 virus in the BALF and nasal washes, and of serum IgG, in mice immunized with hemozoin-adjuvanted inactivated VN1203 virus than in mice immunized with non-adjuvanted inactivated VN1203 virus-immunized mice (Fig. 1B). These results suggest that hemozoin enhanced the mucosal immune responses and

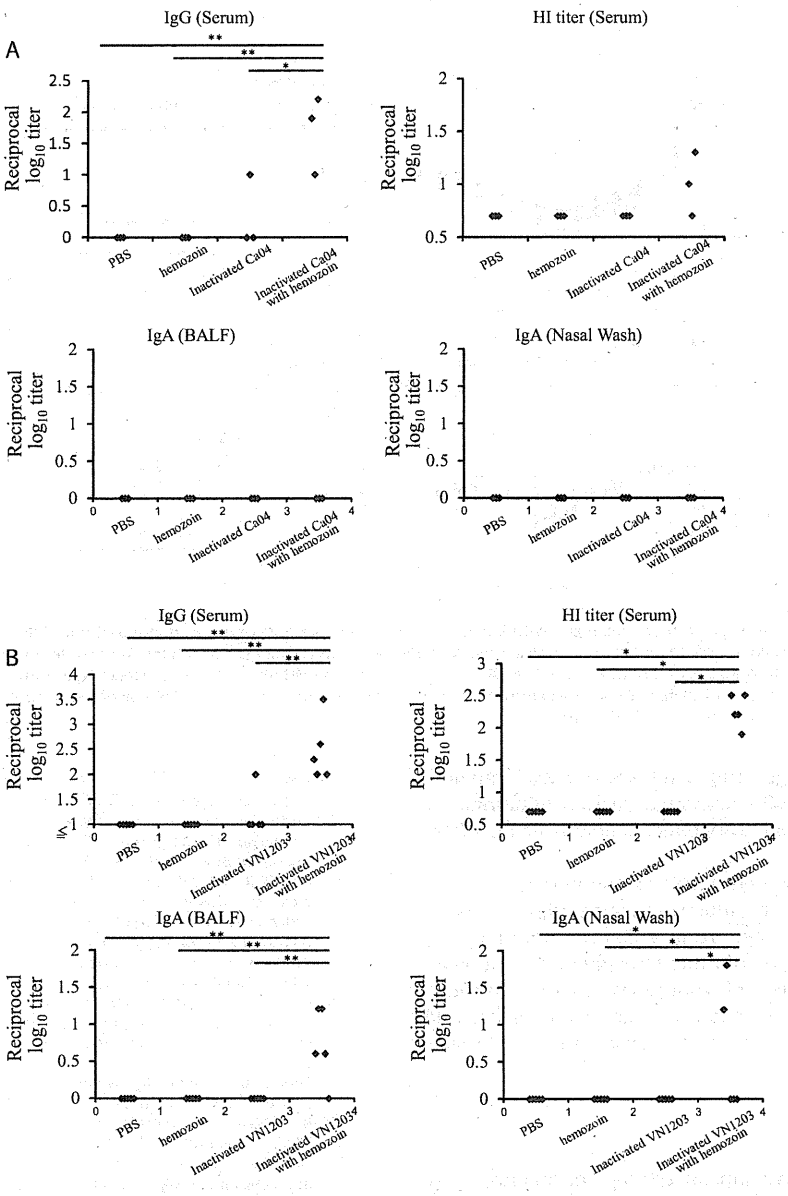


**Fig. 1.** Virus-specific antibody responses in immunized mice. Virus-specific antibodies were detected by means of ELISA and HI assays with purified Ca04 (A) or VN1203 (B) virus as a viral antigen. IgG antibody titers (upper, left panels) and HI titers (upper, right panels) in serum and IgA antibody titers in the BALF (lower, left panels), and nasal washes (lower, right panels) from mice intranasally mock-immunized with PBS or hemozoin or immunized with non-adjuvanted or hemozoin-adjuvanted inactivated virus were measured. Values represent antibody titers in individual mice (A: $n=3$, B: $n=5$). Statistically significant differences (*: $P<0.05$, **: $P<0.01$) are indicated.

may potentially compensate for the well-recognized weakness of inactivated vaccines [30,13,31]. By contrast, enhanced IgA production by the hemozoin addition was not observed with the Ca04 virus counterparts (Fig. 1A). This contradiction may reflect a difference in immunogenicity between the Ca04 and VN1203 viruses. Further study is required to clarify the mechanisms by which hemozoin promotes IgA responses after immunization with inactivated vaccines. In addition, hemozoin-adjuvanted inactivated virus protected mice better than non-adjuvanted inactivated viruses although virus titers in lungs were similar between animals immunized with and without the adjuvant (Fig. 2, Tables 1 and 2). This finding suggests that hemozoin enhanced the vaccine efficacy of the inactivated influenza viruses by modulating host responses. In the current study, we measured viral loads only in respiratory organs, which are the primary sites of influenza virus replication even for strains that cause systemic infection (e.g., VN1203 virus). A further study to examine the inhibitory effect of hemozoin on systemic spread of influenza viruses may explain the better protection afforded by hemozoin-adjuvanted vaccine.

Although hemozoin is a ligand for TLR9 [18–20], studies using TLR9- or MyD88-deficient mice suggest that the potent adjuvant effect of synthetic hemozoin is mediated not via TLR9, but through MyD88 [21]. In addition, previous studies have demonstrated that hemozoin stimulates innate inflammatory responses, inducing neutrophil recruitment via MyD88 [21,32]. Thus, one of the possible mechanisms underlying the hemozoin-mediated enhanced efficacy of inactivated influenza vaccine may be that hemozoin induces the balanced Th1/Th2 responses in a MyD88-dependent manner, leading to the improved immunogenicity of the inactivated influenza viruses and to the better protection against lethal challenge with influenza viruses. Of note, one of four mice administered with only hemozoin survived after the lethal challenge with

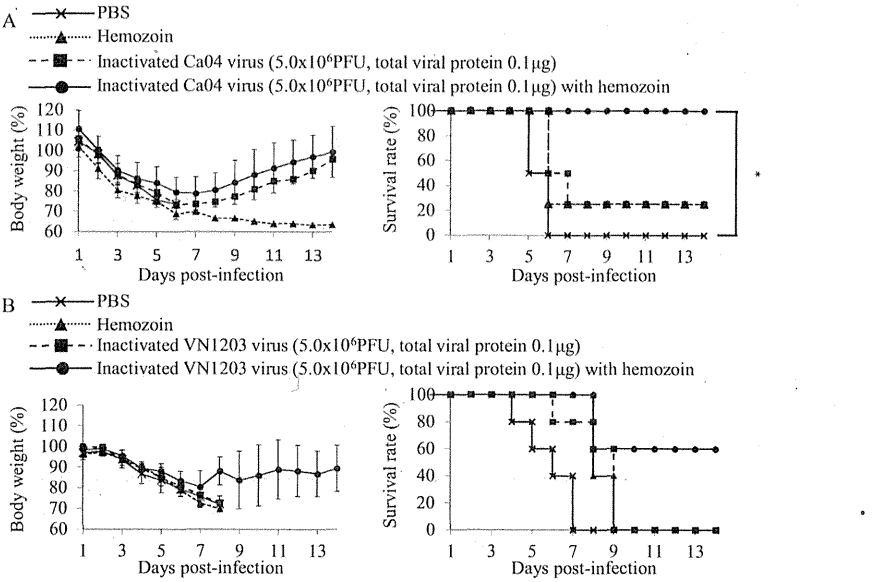


**Fig. 2.** Body weight changes and survival of mice challenged with lethal doses of viruses. Mice were mock-immunized with PBS or hemozoin, or immunized with non-adjuvanted or hemozoin-adjuvanted inactivated virus twice with a 2-week interval in between the immunizations. Three or four weeks after the final immunization, mice were intranasally challenged with 10 $MLD_{50}$ of MACa04 virus (A: $n=4$) or 100 $MLD_{50}$ of VN1203 virus (B: $n=5$), respectively. Body weight (left panels) and survival (right panels) were monitored for 14 days after challenge. Values are expressed as mean changes in body weight ± SD (left panels). Statistically significant differences in the survival rate of immunized mice (*: $P<0.05$) are indicated (A: right panel).

MACa04 virus (Fig. 2A), suggesting that hemozoin itself might have protective effects against influenza virus infection. Additional study is required to clarify the inhibitory effect of hemozoin on influenza virus infection.

In conclusion, here, we demonstrated the potential of hemozoin as a novel whole virion influenza vaccine adjuvant. Because the mechanism by which hemozoin enhances immunogenicity remains unclear, we should continue to evaluate the adjuvanticity of hemozoin in the context of influenza vaccination. In addition, to establish the efficacy of hemozoin as an adjuvant, further studies are needed including studies in an additional animal model such as ferrets.

## Acknowledgements

We thank Dr. Susan Watson for editing the manuscript and Y. Igari and T. Tsukui from Nihon Zenoaq, Co., Ltd. for providing synthetic hemozoin. This work was supported, by a Grant-in-Aid for Specially Promoted Research, by the Japan Initiative for the Global Research Network on Infectious Diseases from the Ministry of Education, Culture, Sports, Science, and Technology, Japan, by grants-in-aid from the Ministry of Health, Labour, and Welfare, Japan, by ERATO (Japan Science and Technology Agency), by Strategic Basic Research Programs of Japan Science and Technology Agency, by National Institute of Allergy and Infectious Diseases Public Health Service research grants, and by an NIAID-funded Center for Research on Influenza Pathogenesis (CRIP, HHSN266200700010C). R.U. is supported by JSPS Research Fellowships for young scientists.

## References

[1] Glezen WP. Cold-adapted, live attenuated influenza vaccine. Expert Rev Vaccines 2004;3(April (2)):131–9.
[2] Neumann G, Kawaoka Y. The first influenza pandemic of the new millennium. Influenza Other Respir Viruses 2011;5(May (3)):157–66.
[3] Nabel GJ, Fauci AS. Induction of unnatural immunity: prospects for a broadly protective universal influenza vaccine. Nat Med 2010;16(December (12)):1389–91.
[4] Lambert LC, Fauci AS. Influenza vaccines for the future. N Engl J Med 2010;363(November (21)):2036–44.
[5] Rimmelzwaan GF, Fouchier RA, Osterhaus AD. Influenza virus-specific cytotoxic T lymphocytes: a correlate of protection and a basis for vaccine development. Curr Opin Biotechnol 2007;18(December (6)):529–36.
[6] Cox RJ, Brokstad KA, Ogra P. Influenza virus: immunity and vaccination strategies. Comparison of the immune response to inactivated and live, attenuated influenza vaccines. Scand J Immunol 2004;59(January (1)):1–15.
[7] Brokstad KA, Cox RJ, Olofsson J, Jonsson R, Haaheim LR. Parenteral influenza vaccination induces a rapid systemic and local immune response. J Infect Dis 1995;171(January (1)):198–203.
[8] Cox RJ, Brokstad KA, Zuckerman MA, Wood JM, Haaheim LR, Oxford JS. An early humoral immune response in peripheral blood following parenteral inactivated influenza vaccination. Vaccine 1994;12(August (11)): 993–9.
[9] Tetsutani K, Ishii KJ. Adjuvants in influenza vaccines. Vaccine 2012; 30(December (52)):7658–61.
[10] Reed SG, Orr MT, Fox CB. Key roles of adjuvants in modern vaccines. Nat Med 2013;19(December (12)):1597–608.
[11] Dey AK, Srivastava IK. Novel adjuvants and delivery systems for enhancing immune responses induced by immunogens. Expert Rev Vaccines 2011;10(February (2)):227–51.
[12] van Riet E, Ainai A, Suzuki T, Hasegawa H. Mucosal IgA responses in influenza virus infections; thoughts for vaccine design. Vaccine 2012;30(August (40)):5893–900.
[13] Tumpey TM, Renshaw M, Clements JD, Katz JM. Mucosal delivery of inactivated influenza vaccine induces B-cell-dependent heterosubtypic cross-protection against lethal influenza A H5N1 virus infection. J Virol 2001;75(June (11)):5141–50.
[14] Ainai A, Tamura S, Suzuki T, Ito R, Asanuma H, Tanimoto T, et al. Characterization of neutralizing antibodies in adults after intranasal vaccination with an inactivated influenza vaccine. J Med Virol 2012;84(February (2)):336–44.
[15] Petrovsky N, Aguilar JC. Vaccine adjuvants: current state and future trends. Immunol Cell Biol 2004;82(October (5)):488–96.
[16] Francis SE, Sullivan Jr DJ, Goldberg DE. Hemoglobin metabolism in the malaria parasite *Plasmodium falciparum*. Annu Rev Microbiol 1997;51: 97–123.
[17] Arese P, Schwarzer E. Malarial pigment (haemozoin): a very active 'inert' substance. Ann Trop Med Parasitol 1997;91(July (5)):501–16.
[18] Coban C, Ishii KJ, Kawai T, Hemmi H, Sato S, Uematsu S, et al. Toll-like receptor 9 mediates innate immune activation by the malaria pigment hemozoin. J Exp Med 2005;201(January (1)):19–25.
[19] Parroche P, Lauw FN, Goutagny N, Latz E, Monks BG, Visintin A, et al. Malaria hemozoin is immunologically inert but radically enhances innate responses by presenting malaria DNA to Toll-like receptor 9. Proc Natl Acad Sci U S A 2007;104(February (6)):1919–24.
[20] Wu X, Gowda NM, Kumar S, Gowda DC. Protein–DNA complex is the exclusive malaria parasite component that activates dendritic cells and triggers innate immune responses. J Immunol 2010;184(April (8)):4338–48.